Mon. Not. R. Astron. Soc. **284,** 839–858 (1997)

Spectroscopic modelling of non-radial pulsation in rotating early-type stars

R. H. D. Townsend*

Department of Physics and Astronomy, University College London, Gower Street, London WC1E 6BT

Accepted 1996 August 21. Received 1996 August 21; in original form 1996 June 10

ABSTRACT

A new computer model which simulates non-radial pulsations in rotating early-type stars is presented. The model constructs time-resolved synthetic spectra for a star undergoing multi-mode non-radial pulsation, using a rotationally distorted stellar grid and intrinsic spectral line profiles calculated from non-LTE model atmospheres. The treatment includes consideration of pulsation-induced velocity fields and temperature, surface-area and surface-normal perturbations. The effects of rotation on the pulsation modes of the star are considered by expressing the perturbed variables as linear combinations of terms proportional to spherical harmonics. Rotation acts to concentrate pulsational activity towards the stellar equator; this equatorial concentration, when combined with gravity darkening, leads to significant differences in the degree of line-profile variability between spectral lines formed at the equator and the pole, for both sectoral *and* tesseral modes. The rotation also leads to the existence of oscillatory quasi-toroidal modes. The use of rotationally modified velocity fields and temperature perturbations leads to significant changes to the calculated line-profile variability. In contrast, the surface-area and surface-normal perturbations are the more important mechanisms for generating continuum variations, emphasizing the need for a proper treatment of these effects in the modelling of photometric variability.

Key words: line: profiles – stars: early-type – stars: oscillations – stars: rotation.

1 INTRODUCTION

Since the discovery of the 'five-minute' solar oscillations (Leighton, Noyes & Simon 1962), the discipline of helioseismology has offered unparalleled insights into the structure and physical characteristics of the solar interior. Such insights have proved invaluable for comparison with theories of stellar evolution. The newly emergent field of asteroseismology represents the logical generalization of pulsation studies from our own star to others, in search of similar detailed constraints on stellar interiors. Over the past twenty years, beginning with the pioneering work of Smith & Karp (1976) and Walker, Yang & Fahlman (1979), time-resolved high-resolution spectroscopy of early-type (O and B) stars has shown that line-profile variations (lpv) appear to be commonplace in such stars (Fullerton, Gies & Bolton 1996). Smith (1977) and Vogt & Penrod (1983) suggested that the lpv observed were due to non-radial pulsation (NRP); more recent studies have supported this hypothesis in some stars (Kambe, Ando & Hirata 1990; Howarth & Reid 1993; Reid et al. 1993; Reid & Howarth 1996).

Theoretical treatments of NRP pre-date most observational studies (Thomson 1863); however, the consideration of the rapid rotation prevalent in many early-type stars, such as the established non-radial pulsators ζ Oph and HD 93521 (Reid et al. 1993; Howarth & Reid 1993), has led to subtleties in the theory which have been handled with some measure of success only in the last fifteen years or so. Ledoux (1951) first considered the effects of rotation on pulsation; however, it was Berthomieu et al. (1978) who initially engaged in a comprehensive treatment of *rapid* rotators. Lee & Saio (1986, 1987, 1989, 1990) substantially expanded upon this treatment, and more recent developments (Lee & Baraffe 1995) have gone even further in the attempt to construct a complete theory of rapidly rotating pulsators. However, theoretical studies only have valuable diagnostic potential when coupled with observations; consequentially, methods are required by which to map the predictions of the theories into observable quantities. Such methods usually equate with computer models which construct synthetic spectra of stars undergoing NRP; the lpv inherent in the resultant spectra may be compared with those observed in an attempt to test the theories and also to constrain input parameters for asteroseismological studies of stellar interiors. A number of such codes have been presented previously (Osaki 1971; Smith 1977; Vogt & Penrod 1983; Pesnell 1985; Kambe & Osaki 1988; Aerts & Waelkens 1993; Schrijvers et al. 1996) to model the velocity fields, and in some cases pulsation-induced temperature variations, of a star undergoing NRP. However, it is apparent that a code implementing more of the recent theoretical developments is required, so that some of the more subtle aspects of lpv may be studied.

*E-mail: rhdt@star.ucl.ac.uk

Accordingly, a new code to model NRP in rapidly rotating stars is presented. The code, named BRUCE, constructs from basic principles a rotating model star, which is then perturbed with NRP fields to produce non-LTE synthetic spectra for comparison with observations. In Section 2, a brief review is made of the theoretical treatment of NRP in rotating stars; Section 3 discusses how the pulsation theory is implemented in BRUCE. Section 4 goes on to describe the equilibrium grid used to model the star, and how it is perturbed, and Section 5 considers how the synthetic spectra are calculated from the stellar grid. Some preliminary results are presented in Section 6, and the findings of the paper are summarized in Section 7.

2 THEORETICAL BACKGROUND

2.1 Treatment of rotation

Solution of the linearized hydrodynamical pulsation equations for non-rotating stars (Unno et al. 1989) shows that the normal modes of pulsation for such a star have an angular dependence proportional to the spherical harmonics Y_l^m (Abramowitz & Stegun 1964), defined here by

$$Y_l^m(\theta,\phi) = (-1)^{(m+|m|)/2}\sqrt{\frac{2l+1}{4\pi}\frac{(l-|m|)}{(l+|m|)}}P_l^{|m|}(\cos\theta)\mathrm{e}^{\mathrm{i}m\phi}, \tag{1}$$

where the associated Legendre polynomials P_l^m are given by

$$P_l^m(z) = \frac{(1-z^2)^{m/2}}{2^l l!}\frac{\mathrm{d}^{l+m}}{\mathrm{d}z^{l+m}}(z^2-1)^l. \tag{2}$$

Note that the normalization of the spherical harmonics varies from author to author, and must be considered when comparing results; for example, velocity amplitudes quoted by Aerts & Waelkens (1993) are a factor of $\sqrt{2\pi}$ *larger* than corresponding amplitudes in this paper. The phase term in equation (1), the so-called *Condon–Shortley* phase (Tinkham 1964), is not strictly necessary, but simplifies the consideration of off-axis modes of pulsation (see Section 3.6).

The inclusion of rotational effects in the equations of pulsation leads to extra terms due to both Coriolis and centrifugal forces (Ledoux 1951). The centrifugal force is conservative and hence may be expressed in terms of the gradient of a scalar potential field; this field combines with the gravitational field to yield an effective gravity. The latitudinally dependent effective gravity distorts the equilibrium stellar structure into an oblate spheroid; the pulsation eigenfrequencies – expressible as integrals over the stellar interior (Tassoul 1980) – are correspondingly altered (Ledoux 1951). However, since the linearized pulsation equations are amenable to expression in a form where the only effect of the centrifugal force term is to modify the equilibrium structure, gross modification of pulsation characteristics is not to be expected (Unno et al. 1989).

The Coriolis force, on the other hand, is dependent on the time-derivative of the local Lagrangian displacement in the corotating frame; accordingly, it plays no part in determining the equilibrium stellar structure (since the Lagrangian displacement is zero in the equilibrium state), but does lead to significant modifications of the pulsation characteristics, including the introduction of new types of waves (Section 3.5, also Unno et al. 1989). Applying the algorism of mode analysis to the Coriolis force modified pulsation equations demonstrates that, unlike the non-rotating case, the normal modes of a rotating star can no longer be written in terms of single spherical harmonics; an interaction occurs which couples together harmonics of the same m but differing l (Lee & Saio 1986), resulting in new normal modes of the form

$$f_{l,m} = \sum_{k=|m|}^{\infty}(\mathbf{F})_{k,l}Y_k^m, \tag{3}$$

where $f_{l,m}$ represents some generalized pulsation variable with mode labels l and m, and $\mathbf{F}$ is a matrix of coupling coefficients to be determined by the theory. The fact that only modes of the same m couple together arises from the axisymmetry of the rotational perturbation. Furthermore, it can be demonstrated (Berthomiew et al. 1978; Lee & Saio 1986) that couplings occur only between modes of the same latitudinal parity about $\theta = \pi/2$ – this is due to the reflectional symmetry through the $\theta = \pi/2$ plane of the rotating star. Following the nomenclature of Lee & Saio (1990), hereinafter LS, it is useful to replace l by l_j, and introduce n_j, both of which are defined by

$$\begin{cases} l_j = |m| + 2(j-1), & n_j = |m| + 2(j-1) + 1 \quad \text{(even-parity modes)}, \\ l_j = |m| + 2(j-1) + 1, & n_j = |m| + 2(j-1) \quad \text{(odd-parity modes)}, \end{cases} \tag{4}$$

where j is an integer which takes values upwards from unity.

Berthomieu et al. (1978) first considered applying the so-called *traditional approximation* (e.g. LS) to rotating stars in an attempt to simplify the theoretical framework used to describe pulsations in such stars. In the traditional approximation, the horizontal (i.e. non-radial) components of the axial rotation vector $\boldsymbol{\Omega}$ are neglected; such an approach is valid for low-frequency pulsations. They substituted expressions of the form of (3) into the pulsation equations to yield two infinite sets of coupled first-order differential equations. Under both the traditional approximation and the Cowling (1941) approximation, where the perturbation to the gravitational potential is neglected, the equations are amenable to expression in vector form (Lee & Saio 1987) in which the coupling between modes is wholly described by a matrix $\mathbf{W}$ of infinite dimension. This matrix is a function of $\nu \equiv 2\Omega/\omega$, where $\Omega \equiv |\boldsymbol{\Omega}|$ is the angular frequency of rotation and ω is the angular frequency of pulsation

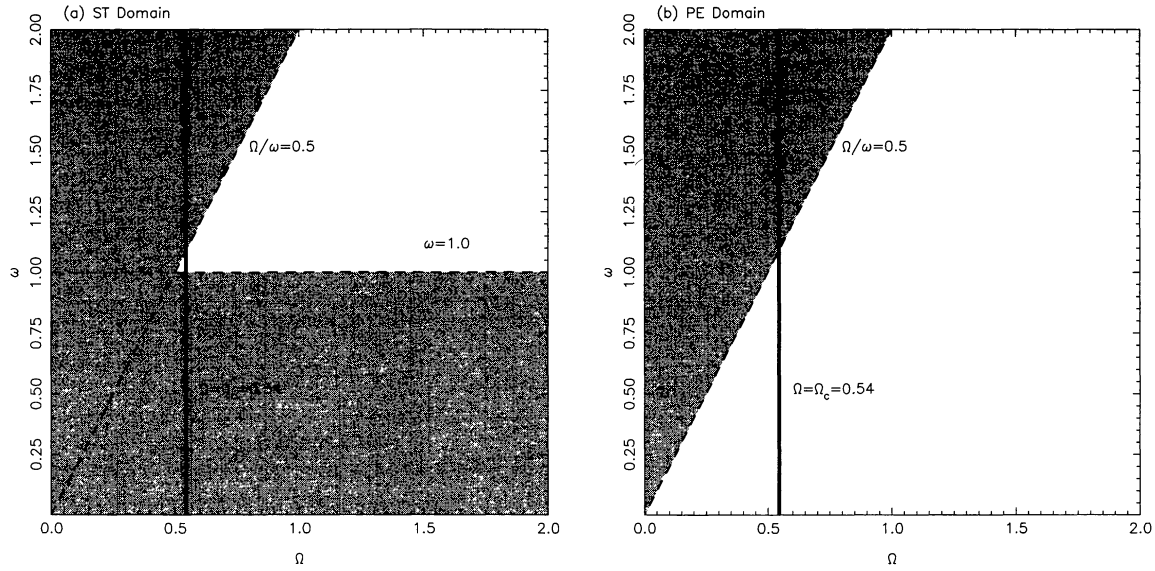

Figure 1. A comparison of the domains of applicability of the (a) ST and (b) PE techniques. The domains are plotted as grey regions in the $\Omega - \omega$ plane; the thick vertical line in each diagram represents the upper limit Ω_c at which the rotation becomes critical. All frequencies are normalized by $(R^3/GM)^{1/2}$.

in the corotating frame of reference; a different matrix exists for each value of m and for the two types of parity. An expression for the components of the inverse matrix $\mathbf{W}^{-1}$, hereinafter denoted $\aleph$, is given by Lee & Saio (1987); they remark that their expression is valid for even modes, although it can be shown (Appendix A) that the expression may be extended to odd modes as well.

Berthomieu et al. (1978) demonstrated that, by applying a similarity transformation to the two sets of equations, $\mathbf{W}$ may be brought into a diagonal form $\mathbf{D}$, thus decomposing the system into pairs of ordinary, uncoupled differential equations. These equations have a functional form identical to that of the non-rotating pulsation equations, with the replacement of a term $l(l+1)$ by $\lambda_{l,m}$ (LS); $\lambda_{l,m}$ is one of the diagonal components of $\mathbf{D}$, and is therefore an eigenvalue of $\mathbf{W}$. The decoupling of the equations is equivalent to a transformation from the spherical harmonic basis Y_l^m to a new basis set, denoted by $|\lambda_{l,m}\rangle$ (following LS), which forms the normal mode set for rotating stars. BRUCE uses this new basis set to calculate the velocity fields on the surface of a rotating star; a discussion of this implementation of the theories of Berthomieu et al. (1978) and LS, along with some extensions to the theory, appears in Section 3.

2.2 Domain of applicability

The similarity transformation technique (hereinafter ST) described herein is radically different from the perturbation-expansion formalism (hereinafter PE) first used by Ledoux (1951) and more recently by other authors (Saio 1981; Martens & Smeyers 1982; Aerts & Waelkens 1993; Schrijvers et al. 1996). PE techniques rely on expressing the rotationally modified pulsation variables as truncated (usually to first order) power series in Ω/ω (strictly, the zero-rotation frequency ω_0 is used rather than the rotationally modified ω, but the difference between the two may be neglected for small Ω/ω); it is evident that such expressions will, in general, diverge for Ω/ω greater than unity, which limits the applicability of PE techniques to high-frequency p-modes and slowly rotating stars. Many authors (Aerts & Waelkens 1993; Schrijvers et al. 1996) limit their first-order expressions to $\Omega/\omega < 0.5$, which proves insufficient for the treatment of low-frequency g-modes and/or rapidly rotating stars. However, PE techniques continue to be successful for the treatment of higher-frequency p-modes.

In contrast, ST has a somewhat broader domain of applicability. To discuss this, it is useful to introduce the dimensionless pulsation frequency $\bar{\omega}$, given by

$$\bar{\omega} = \sqrt{\frac{\omega^2 R^3}{GM}}, \tag{5}$$

where R and M are the stellar radius and mass respectively. For low-frequency oscillations ($\bar{\omega} < 1$), corresponding to g-modes, second- and higher-order terms originating from the Coriolis force dominate the effects of centrifugal force on the equilibrium structure (Unno et al. 1989). Within the traditional approximation (which implicitly neglects the effects of the centrifugal force) and the Cowling approximation, ST provides a *complete* treatment of the Coriolis force; it does *not* rely on any power-series expansions and hence may be used for *all* values of Ω/ω. However, when $m = 0$, the matrix $\aleph$ has singular components, and $\mathbf{W}$ must be used in its place – this increases the complexity of the ST formulation. Furthermore, Clement (1981) demonstrated that, for axisymmetric ($m = 0$) modes, second-order (centrifugal) terms are as important as those of first order, so it is questionable whether ST *or* PE can be applied to such modes. First-order PE methods have similar problems; other approaches (Clement 1981) must be used to treat $m = 0$ systems.

For higher-frequency oscillations ($\tilde{\omega} > 1$), corresponding to p-modes, ST must be limited to small (typically $\lesssim 0.5$) values of Ω/ω due to the limitations of the traditional approximation – indeed, PE is possibly more accurate than ST methods for the treatment of high-frequency p-modes. However, for a stable star, Ω does not exceed the critical rotation value $\Omega_c = (8GM/27R^3)^{1/2}$, at which the effective gravity at the equator tends to zero. Combining this upper limit on Ω with the heuristic $\tilde{\omega} > 1$ lower boundary for p-mode oscillations leads to a *physical* upper limit of $\Omega/\omega \lesssim 0.54$ in the p-mode domain, which serendipitously coincides with the applicability boundary of the theory. Thus ST appears to be applicable in all *physically realistic* regions of $\Omega - \omega$ space; this result is summarized in Fig. 1.

3 IMPLEMENTATION

3.1 Basic expressions

LS demonstrate that the velocity field at the surface of a rotating star due to the excitation of a single pulsation mode may be written as

$$\boldsymbol{v}_{\rm osc} = A\Re\left\{\left[|\lambda_{l_j,m}\rangle\hat{\boldsymbol{r}} + K\left(\nabla_h \sum_{k=1}^{\infty}(\boldsymbol{h}_j)_k|\lambda_{l_k j}\rangle + \nabla_h \times \sum_{k=1}^{\infty}(-\mathrm{i}\boldsymbol{t}_j)_k|\lambda_{n_k j}\rangle\hat{\boldsymbol{r}}\right)\right]\mathrm{e}^{\mathrm{i}\omega t}\right\}, \tag{6}$$

where $\hat{\boldsymbol{r}}$ is the unit radial vector, $\Re$ denotes the real part, and the other symbols have the same meanings as those defined by LS. The velocity amplitude A is, in fact, the rms velocity amplitude normalized over the surface of the star; its relation to the maximum velocity amplitude at the surface depends upon l_j, m and ν in a complicated way. Both l_j and m act as 'labels' for the pulsation mode; even though l_j is no longer a 'good' eigenvalue, it is still possible to refer to eigenstates by the l_j (and of course m) of the spherical harmonic that they correspond to in the zero-rotation limit (e.g. LS). Although the pulsation frequency ω is modified by the rotation (Ledoux 1951), in equation (6) ω is taken to be a free parameter, and thus rotational modifications to ω are treated implicitly. The variable K, equal to $1/\tilde{\omega}^2$, is implicitly modified by rotation through these modifications to ω; this is in contrast to the explicit modifications to K which Schrijvers et al. (1996) incorporate in their expressions.

The new basis states $|\lambda_{l_j,m}\rangle$ form a complete orthonormal set over the surface of a sphere, and are given in terms of spherical harmonics by the expression

$$|\lambda_{l_j,m}\rangle = \sum_{k=1}^{\infty}(\mathbf{B})_{kj}Y_{l_k}^m, \tag{7}$$

where $\mathbf{B}$ is the orthogonal matrix used to effect the similarity transformation and bring $\mathbf{W}$ into diagonal form; the column vectors of $\mathbf{B}$ are the eigenvectors of $\mathbf{W}$. In any realistic implementation, the upper limit of the sum in equation (7) must be taken at some large but finite value N; this truncation obviously introduces some unwanted side-effects, but for suitably large N these side-effects are negligible (Berthomieu et al. 1978; Lee & Saio 1989). Throughout this paper, N is taken to be 100; this value was chosen since it yielded the same results as sums with larger ($\geq$200) numbers of terms, yet allowed calculations to be performed on reasonable time-scales.

Although $N = 100$ summations include terms up to $l_j \sim 200$, the summation terms do not manifest themselves as individual, distinguishable modes in the lpv of the model star; rather, they combine to modify the gross characteristics of a single mode. It is important to include many low-amplitude, high-l_j terms in the summations to preserve the smoothness of the rotationally modified modes; otherwise, artificial 'ringing' features will appear in the modified modes, akin to the Gibbs-phenomenon oscillations (Arkfen 1970) apparent in the truncated Fourier-series expansion of, for example, a square wave. First-order PE techniques (Aerts & Waelkens 1993; Schrijvers et al. 1996), which use only three spherical harmonic terms to model pulsation, may introduce erroneous structure into the rotationally modified modes for this reason. It must be stressed that empirical line-profile variation analysis is not specifically tuned to the detection of spherical harmonics above other pulsation-mode morphologies, so such analysis will never detect the individual terms in expressions like equation (7); rather, it will detect the gross characteristics of the modified modes, such as the number of nodal lines on the surface.

It is useful to observe that the inverse matrix $\aleph$ shares the same set of eigenvectors as $\mathbf{W}$, and has eigenvalues reciprocal to those of $\mathbf{W}$: if $\boldsymbol{b}_j$ denotes the eigenvector corresponding to the eigenstate $|\lambda_{l_j,m}\rangle$ with components given by

$$(\boldsymbol{b}_j)_k = (\mathbf{B})_{k,j}, \tag{8}$$

then it is possible to write

$$\aleph\boldsymbol{b}_j = \lambda_{l_j,m}^{-1}\boldsymbol{b}_j. \tag{9}$$

Since expressions for the components of $\aleph$ are available in closed form (Appendix A), it is computationally efficient to use $\aleph$ in place of $\mathbf{W}$ for calculations using the new basis states; accordingly, BRUCE uses $\aleph$ throughout, converting between the eigenvalues of $\aleph$ and those of $\mathbf{W}$ where necessary. A discussion of the techniques used for the diagonalization and manipulation of $\aleph$ follows in the next section; details of how equation (6) is implemented can be found in Section 3.3.

3.2 Matrix reductions

The matrix $\aleph$ is symmetric and tridiagonal, properties which lend themselves well to numerical manipulation. The method used to find the eigenvectors of this matrix is a QL-type algorithm with implicit shifts (Press et al. 1992) which has a very low operation count ($\sim 3N^3$ to find all eigenvalues and all eigenvectors), and is guaranteed to converge for a matrix of this type. However, the algorithm produces eigenvalue/eigenvector

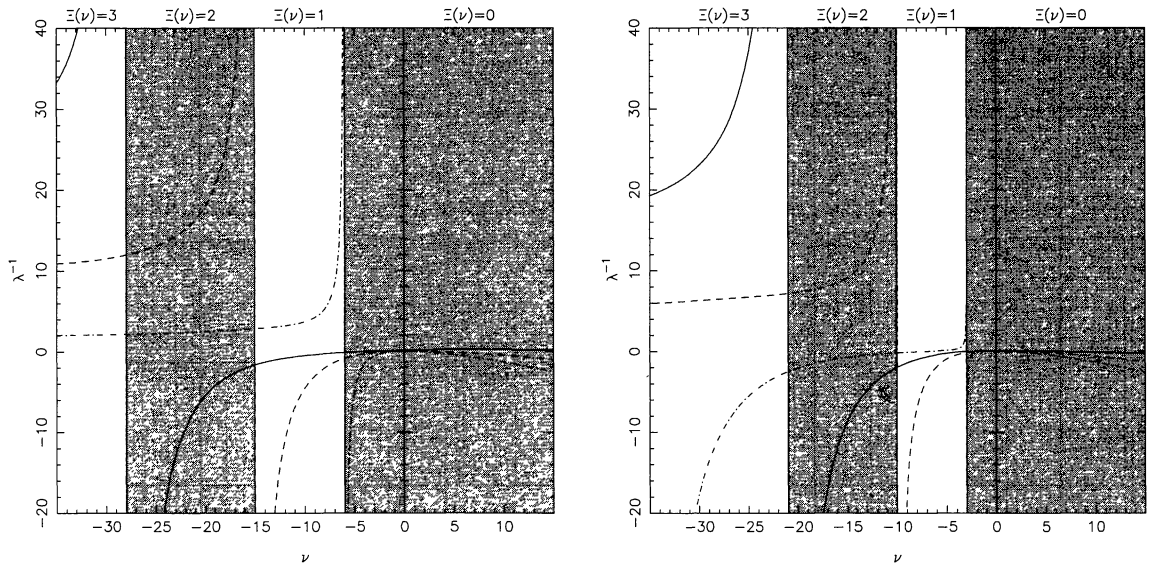

Figure 2. A graph of the eigenvalues λ^{-1} of the matrix $\aleph$ as a function of rotation parameter ν for the $m = -2$ even (left panel) and odd (right panel) parity modes. The matrix dimension N was taken to be 3, and the $j = 1, 2, 3$ eigenvalues are plotted as solid, dashed and dot-dash curves respectively. The shading demarcates regions of differing $\Xi(\nu)$; at the boundaries of these regions, one of the three eigenvalues is singular, and the positive-to-negative ordering of the eigenvalues is permuted cyclically once. The $\lambda^{-1} = 0$ axis has been omitted for clarity.

pairs without the l–m labelling required to identify which eigenvalue/eigenvector pairs correspond to which pulsation modes. It is therefore necessary to develop a procedure by which the modes may be identified.

Except in the zero-rotation limit, $\aleph$ is unreduced – that is, all components adjacent to the diagonal remain non-zero. If $\mathbf{C}(x)$ denotes the matrix $(\aleph - x\mathbf{I})$, where $\mathbf{I}$ is the identity matrix of dimension N, then it can be observed that the first $N-1$ columns of $\mathbf{C}(x)$ form a set of $N-1$ linearly independent vectors. Accordingly, the rank of $\mathbf{C}(x)$ *by definition* is at least $N-1$. By the spectral theorem (Parlett 1980), the rank R of a matrix plus the nullity E must equal the dimension N; thus

$$R + E = N,\ R \geq N-1 \longrightarrow E = \begin{cases} 0 & (x \text{ is not an eigenvalue of } \aleph), \\ 1 & (x \text{ is an eigenvalue of } \aleph). \end{cases} \tag{10}$$

The nullity E is therefore at maximum 1, and accordingly there can only be one independent eigenvector per eigenvalue. From this one can conclude that the eigenvalues of $\aleph$ are all distinct. Now, in the zero-rotation limit the eigenvalues $\lambda^{-1}_{l,m}$ are given by

$$\lambda^{-1}_{l_j,m} = \frac{1}{\Lambda(l_j)}, \tag{11}$$

where $\Lambda(x) \equiv x(x+1)$; it is apparent that the eigenvalues have a well defined positive-to-negative ordering with respect to j. As the rotation parameter ν is varied smoothly from zero, the fact that the eigenvalues are distinct means that the only mechanism by which this ordering may be changed is by a singularity in the behaviour of one of the eigenvalues with respect to ν. Such singularities occur when the components of $\aleph$ have poles; it can be demonstrated that, when $m\nu = \Lambda(n_j)$, four components $[(\aleph)_{j,j}$, $(\aleph)_{j,j\pm1}$, $(\aleph)_{j\pm1,j}$ and $\aleph_{j\pm1,j\pm1}$ for even (+) and odd (−) modes] exhibit regular poles, and the most negative eigenvalue tends to $-\infty$ as ν approaches the singular point ν_s from $|\nu| < |\nu_s|$. For $|\nu| > |\nu_s|$, the same eigenvalue becomes the most positive; the positive-to-negative ordering of the eigenvalues has been permuted cyclically once.

It is now apparent that mode identification is a relatively simple task. Let $\Xi(\nu')$ represent the number of singular points ν_s falling between $\nu = \nu'$ and $\nu = 0$; the positive-to-negative ordering of the eigenvalues at $\nu = \nu'$ is then given by the sequence $j = 1, 2, 3, \ldots, N$ permuted cyclically $\Xi(\nu')$ times *to the right* (i.e. $j = 1, 2, 3, \ldots, N \longrightarrow j = N, 1, 2, \ldots, N-1 \longrightarrow j = N-1, N, 1, \ldots, N-2$). Given a full set of eigenvalues for known ν and m, calculating $\Xi(\nu)$ is trivial, and correct values of j may be assigned to the eigenvalues (and to their corresponding eigenvectors). This procedure is best illustrated in Fig. 2, which shows the eigenvalues of $\aleph$ for a matrix dimension N of 3; zones of differing $\Xi(\nu)$ are alternately shaded, and it is apparent that adjacent zones have eigenvalue orderings which differ by a single cyclic permutation. BRUCE implements such a procedure to identify correctly the eigenvalue/eigenvector pairs produced by the QL matrix-diagonalization algorithm.

3.3 Constructing the velocity fields

The velocity fields described in the preceding section are implemented within BRUCE via an algorithm designed to take full advantage of any symmetries inherent in the model star. The algorithm is built around a *stable* recurrence relation used to generate the associated Legendre

polynomials (Abramowitz & Stegun 1964), namely

$$(l-m)P_l^m(z) = z(2l-1)P_{l-1}^m(z) - (l+m-1)P_{l-2}^m, \tag{12}$$

where the recurrence relation is initiated using the expression

$$P_m^m(z) = (-1)^m(2m-1)!!(1-z^2)^{m/2}, \tag{13}$$

and the notation $n!!$ denotes the product of all *odd* positive integers less than or equal to n. This relation is particularly suited to the task at hand, since the implementation of equation (7) requires a sequence of associated Legendre polynomials of equal m and l taking values from $|m|$ upwards.

Direct implementation of equation (6) proves to be computationally inefficient, since calculation of the horizontal velocity fields involves two N-term summations, one to construct $|\lambda_{l_j,m}\rangle$ from the spherical harmonics, and a second over k to evaluate the horizontal terms, leading to a computation cost of order $\sim 2N^2 + N$. Accordingly, BRUCE constructs two secondary bases $|\eta_{l_j,m}\rangle$ and $|\tau_{n_j,m}\rangle$ defined by the relations

$$|\eta_{l_j,m}\rangle = \sum_{k=1}^{N} (\mathbf{Q})_{k,j} Y_{l_k}^m, \tag{14}$$

and

$$|\tau_{n_j,m}\rangle = \sum_{k=1}^{N} (\mathbf{R})_{k,j} Y_{n_k}^m, \tag{15}$$

where the matrix $\mathbf{Q}$, of dimension N, has components given by

$$(\mathbf{Q})_{k,j} = \frac{\lambda_{l_j,m}}{\Lambda(l_k)} (\boldsymbol{b}_j)_k, \tag{16}$$

and the matrix $\mathbf{R}$, also of dimension N, has components given by

$$(\mathbf{R})_{k,j} = \frac{\nu\lambda_{l_j,m}}{1 - m\nu/\Lambda(n_k)} \left[\frac{J_{n_k}^m}{n_k^2} (\boldsymbol{b}_j)_k + \frac{J_{n_k+1}^m}{(n_k+1)^2} (\boldsymbol{b}_j)_{k+1} \right], \tag{17}$$

for even modes, and by

$$(\mathbf{R})_{k,j} = \frac{\nu\lambda_{l_j,m}}{1 - m\nu/\Lambda(n_k)} \left[\frac{J_{n_k+1}^m}{(n_k+1)^2} (\boldsymbol{b}_j)_k + \frac{J_{n_k}^m}{n_k^2} (\boldsymbol{b}_j)_{k-1} \right] \tag{18}$$

for odd modes. The symbols used in equations (17) and (18) have the same meanings as those of LS. With $|\eta_{l_j,m}\rangle$ and $|\tau_{n_j,m}\rangle$ so defined, $\boldsymbol{v}_{\rm osc}$ is then given by

$$\boldsymbol{v}_{\rm osc} = A\Re\left\{ \left[|\lambda_{l_j,m}\rangle \hat{\boldsymbol{r}} + K\left(\nabla_h |\eta_{l_j,m}\rangle - \mathrm{i}\nabla_h \times |\tau_{n_j,m}\rangle \hat{\boldsymbol{r}} \right) \right] \mathrm{e}^{\mathrm{i}\omega t} \right\}, \tag{19}$$

which has a much-reduced computation cost of order $\sim 3N$. A further reduction in the amount of work involved in calculating $\boldsymbol{v}_{\rm osc}$ arises from the fact that, for a given mode, the pulsational velocity is a product of a function of θ alone and a function of ϕ and t together. Thus the part of $\boldsymbol{v}_{\rm osc}$ dependent on θ alone need be calculated once and once only for a given mode. Furthermore, since, even in a rotating star, the normal modes still have a definite parity about $\theta = \pi/2$, $\boldsymbol{v}_{\rm osc}$ need only be evaluated for θ covering one hemisphere of the star; values in the other hemisphere can then be trivially found by considering the parity of the mode in question.

To demonstrate the effects of rotation on the pulsation modes, the radial eigenfunctions $|\lambda_{l_j,m}\rangle$ for $l_j = 8$ and various values of m are plotted as functions of $\cos\theta$ and ν in Fig. 3. In these diagrams, ϕ is taken to be zero. It is at once apparent that, as discussed by LS, the effect of rotation is to *compress* pulsation activity towards the equator ($\cos\theta = 0$), and to introduce an extra latitudinal node *per hemisphere* in the retrograde ($\nu < 0$) modes; furthermore, the effects of rotation at a given $|\nu|$ are more appreciable for retrograde modes than for prograde modes. The introduction of the two extra latitudinal nodes in the retrograde case could lead, in a star with sufficiently large $|\nu|$, to the misidentification of a retrograde sectoral mode as an $l = |m| + 2$ tesseral mode; in any case, the additional nodes will lead to large cancellation effects when such a star is viewed equator-on. It is apparent that, for high $(l - |m|)$ tesseral modes, the rotational compression is quite severe for $|\nu| \gtrsim 1$; the rotation dramatically alters the characteristics of the pulsation modes, underlining the requirement for suitably large N discussed in Section 3.1. Such compression, when coupled with gravity darkening, will lead to strong lpv in equatorially formed absorption lines, but correspondingly weak lpv in lines formed at the poles (Section 4.1).

3.4 First-order expressions

To allow comparison with other treatments, it is useful to find an expression for $\boldsymbol{v}_{\rm osc}$ correct to first order in ν. In the first-order limit, $\aleph$ is diagonal, with components given by

$$(\aleph)_{j,j} = \left[1 - \frac{m\nu}{\Lambda(l_j)} \right] \Big/ \Lambda(l_j). \tag{20}$$

Hence **W** has eigenvalues given by

$$\lambda_{l_j,m} = \Lambda(l_j) + m\nu, \tag{21}$$

and the eigenvector matrix **B** is the unit matrix **I**. The expressions for the new basis states $|\lambda_{l_j,m}\rangle$, $|\eta_{l_j,m}\rangle$ and $|\tau_{n_j,m}\rangle$ of equation (19) are then, to first order in ν,

$$|\lambda_{l_j,m}\rangle = Y^m_{l_j}, \tag{22}$$

$$|\eta_{l_j,m}\rangle = \left[1 + \frac{m\nu}{\Lambda(l_j)}\right] Y^m_{l_j}, \tag{23}$$

and

$$|\tau_{n_j,m}\rangle = \nu\left[\frac{l_j+1}{l_j} J^m_{l_j} Y^m_{l_j-1} + \frac{l_j}{l_j+1} J^m_{l_j+1} Y^m_{l_j+1}\right], \tag{24}$$

where the symbol J^m_l is defined by LS. These expressions should be contrasted with zeroth-order expressions appropriate for non-rotating stars; it is apparent that, as reported by other authors (Aerts & Waelkens 1993; Schrijvers et al. 1996), the action of the rotation, to first order, is to mix into the zeroth-order expressions one spheroidal and two toroidal terms. Equations (22), (23) and (24) should be compared with similar expressions found by PE techniques. Aerts & Waelkens (1993) use a first-order PE method; however, owing to an couple of typographical errors in that paper,[1] the more recent work of Schrijvers et al. (1996), based on the former paper, is used for comparison herein. Schrijvers et al. (1996), using a first-order PE technique, find for the toroidal basis states the expression

$$|\tau_{l,m}\rangle = \nu\left\{\frac{l+|m|}{l(2l+1)}\frac{[1+(l+1)K]}{K}\sqrt{\frac{(l-|m|)(2l+1)}{(l+|m|)(2l-1)}} Y^m_{l-1} + \frac{l-|m|+1}{(l+1)(2l+1)}\frac{(1-lK)}{K}\sqrt{\frac{(l+|m|+1)(2l+1)}{(l-|m|+1)(2l+3)}} Y^m_{l+1}\right\}, \tag{25}$$

where the expressions under the radicals are to convert from the unnormalized spherical harmonics, used by Schrijvers et al. (1996), to the normalized ones used in this paper. The j-subscripts have been dropped since, to first order, there is essentially no functional distinction between even and odd modes. Because the equations (22), (23) and (24) are strictly valid only in the low-frequency (high-K) domain, it is assumed that $K \gg 1$, to give equation (25) as

$$|\tau_{l,m}\rangle = \nu\left[\frac{l+1}{l}\sqrt{\frac{(l-|m|)(l+|m|)}{(2l-1)(2l+1)}} Y^m_{l-1} + \frac{l}{l+1}\sqrt{\frac{(l-|m|+1)(l+|m|+1)}{(2l+1)(2l+3)}} Y^m_{l+1}\right], \tag{26}$$

which may be further simplified to

$$|\tau_{l,m}\rangle = \nu\left[\frac{l+1}{l} J^m_l Y^m_{l-1} + \frac{l}{l+1} J^m_{l+1} Y^m_{l+1}\right]. \tag{27}$$

This result is the same as equation (24); it can be shown that the expressions for the spheroidal correction term are in accord also. Thus, to first order in the low-frequency domain, the ST and PE techniques are in full agreement. For higher-frequency modes, this agreement breaks down, since the condition that $K \gg 1$ no longer holds; however, ν is generally small for such modes, and so all correction terms are small; any discrepancy between ST and PE for high-frequency modes will therefore be correspondingly small.

3.5 Quasi-toroidal modes

Near the singular points $m\nu = \Lambda(n_j)$ discussed in Section 3.2, the velocity fields $v_{\rm osc}$ of a pulsating star are dominated by horizontal toroidal terms arising from the toroidal basis state $|\tau_{n_j,m}\rangle$, which is in turn dominated by a single spherical harmonic $Y^m_{n_j}$. Such modes are usually termed *quasi-toroidal* (Saio 1982) due to their similarity to the (time-independent) toroidal velocity fields found as trivial solutions of the pulsation equations in non-rotating stars. The effect of rotation is to introduce a time-dependence into the toroidal modes; the co-rotating frequency $\omega_{\rm t}$ of these quasi-toroidal modes may be found by considering that, if

$$m\nu = \Lambda(n_j), \tag{28}$$

and $\nu \equiv 2\Omega/\omega$, then

$$\omega_{\rm t} = \frac{2m\Omega}{\Lambda(n_j)}, \tag{29}$$

which is the result found by Papaloizou & Pringle (1978) for quasi-toroidal modes in slowly rotating stars; inspection of equation (29) shows that the quasi-toroidal modes are retrograde in the corotating frame of reference. It is thus demonstrated that quasi-toroidal modes appear naturally when the Coriolis force is included in the equations of pulsation.

[1]The azimuthal velocity fields have been omitted from their expression (19) for the pulsational velocity fields; see also Aerts & Waelkens (1995).

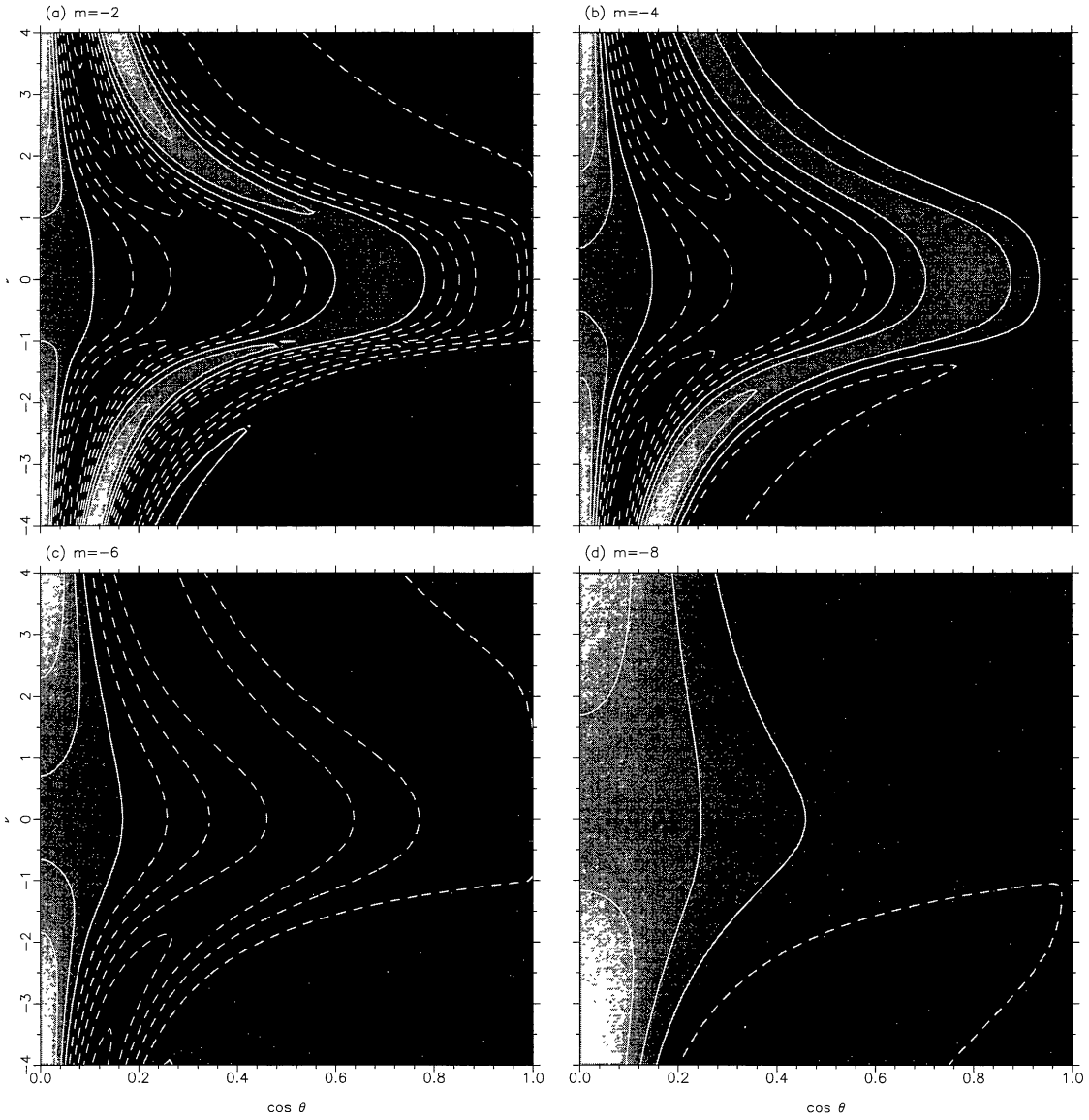

Figure 3. Contour/grey-scale plots of the rotationally modified pulsation eigenfunctions $|\lambda_{l_j,m}\rangle$ as a function of $\cos\theta$ and rotation parameter $\nu \equiv 2\Omega/\omega$ for $l_j = 8$ and $-m = 2$, 4, 6 and 8 (i.e. even modes). The contours are equally spaced at (arbitrary) intervals of 0.08; solid and dashed contours represent $|\lambda_{l_j,m}\rangle > 0$ and $|\lambda_{l_j,m}\rangle < 0$ respectively. Note the extra latitudinal node at the bottom of each panel, introduced by retrograde ($\nu < 0$) pulsation.

3.6 Off-axis modes

It is possible that in some stars, the axis of pulsation (i.e. the axis with respect to which the spherical harmonics are defined) does not coincide with the axis of rotation. Such a phenomenon is thought to occur in Ap stars with strong magnetic fields (Kurtz 1982), and may occur in early-type stars. To allow the consideration of such modes, group theory may be used to transform spherical harmonics off the rotation axis and around the surface of the star. A spherical harmonic $\tilde{Y}_l^m$ rotated by an angle β around the y-axis (with the convention that positive β rotates the positive z-axis into the positive x-axis) may be written in terms of unrotated spherical harmonics as

$$\tilde{Y}_l^m(\theta,\phi) = \sum_{m'=-l}^{l} (\mathbf{D}^{(l)})_{m',m}(0,\beta,0) Y_l^{m'}(\theta,\phi), \tag{30}$$

where $\mathbf{D}^{(l)}$ is the irreducible matrix representation of the full rotation group of dimension $(2l+1)$. Expressions for the components of $\mathbf{D}^{(l)}$ are given by Tinkham (1964; the expressions assume that the spherical harmonics are constructed with the Condon–Shortley phase convention discussed in Section 2). Use of equation (30) thus allows the implementation of off-axis modes.

Accordingly, for each mode present in the model pulsating star, BRUCE calculates the θ-dependence of $v_{\rm osc}$ using equations (12), (13), (19) and (30), and then combines the results with the ϕ- and t-dependence of equation (19) to generate a sequence of velocity fields for the pulsating

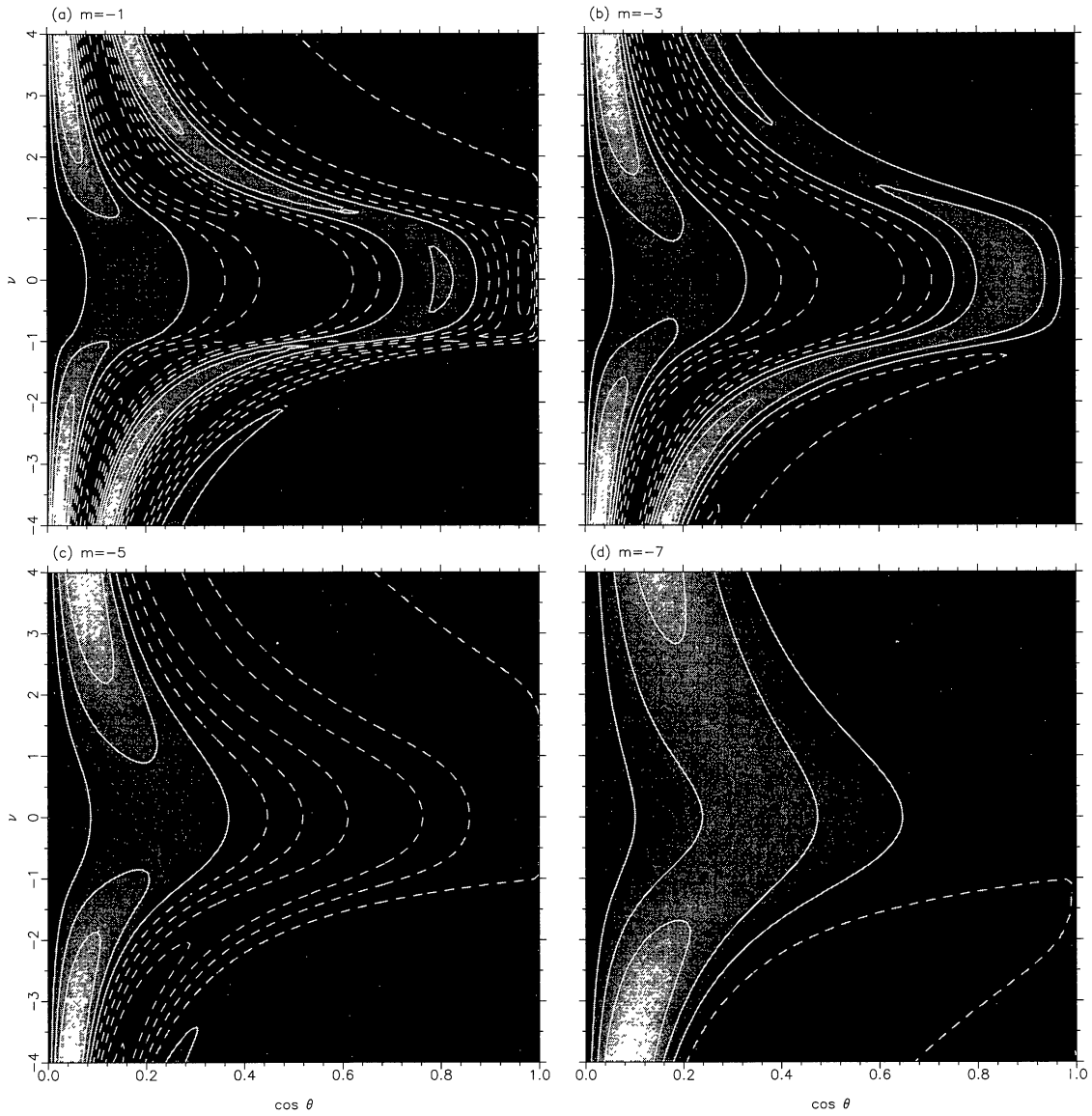

Figure 3 – *continued.* Contour/grey-scale plots of the radial eigenfunctions $|\lambda_{l_j,m}\rangle$ as a function of $\cos\theta$ and ν for $l_j = 8$ and $-m = 1, 3, 5$ and 7 (i.e. odd modes). Again, retrograde ($\nu < 0$) pulsation leads to the introduction of an extra latitudinal node.

star. For these velocity fields to have any physical meaning, they must be applied to some form of rotationally modified stellar grid to produce a complete model star. The following section considers the stellar grid used by BRUCE.

4 STELLAR GRID

4.1 Equilibrium configuration

The stellar grid upon which the velocity fields are overlaid may be implemented in a number of ways. Some authors (Pesnell 1985; Aerts & Waelkens 1993) use a 'semi-analytical' approach whereby an expression for the observables as a function of position on the stellar disc is obtained, and then used to calculate synthetic spectra for the star. This approach suffers from the drawback that implementations for anything other than a spherical star are non-trivial. Accordingly, BRUCE uses a two-dimensional grid wrapped around the entire surface of the star, with the appropriate stellar radius and photospheric physical quantities assigned to each grid point. Although this approach leads to a certain amount of redundancy (i.e. calculations made for non-visible grid points), it is far more flexible than semi-analytical approaches and also more representative of the star itself as a physical entity.

The equilibrium stellar grid, describing the state of the star before any pulsation fields have been applied to it, is uniquely defined in the uniform-rotation approximation by the polar temperature T_p, the polar gravity g_p, the polar radius R_p and the azimuthal rotation velocity at the equator V_{eq}. The equatorial radius R_{eq} of the star is found by assuming that both the pole and the equator lie on the same equipotential surface of

the effective gravitational potential function Φ, given in the Roche model (Collins & Harrington 1966) by

$$\Phi = -\frac{GM}{R} - \frac{1}{2}\Omega^2 R^2 \sin^2\theta, \tag{31}$$

where M is the mass of the star, calculated from g_p and R_p, and the other symbols have their usual meanings. Corrections to this geometry due to radiation pressure may be included by replacing M by a 'reduced mass'. Noting that at the equator $\Omega = V_{eq}/R_{eq}$, one may equate Φ at the pole and the equator to give the equatorial radius as

$$R_{eq} = GM \Big/ \left(\frac{GM}{R_p} - \frac{{V_{eq}}^2}{2}\right). \tag{32}$$

With the equatorial radius so defined, it is possible to calculate Ω. Solution of equation (31) is then achieved using a Newton–Raphson algorithm, which calculates the surface radius $R(\theta)$ of the star at various colatitudes θ to a user-definable fractional tolerance (taken to be 10^{-6} throughout this paper).

The size of the stellar grid is governed by N_{eq}, the number of grid points lying along the equator. At a colatitude θ, there are approximately $N_{eq}\sin\theta$ grid points arrayed in a ring perpendicular to the rotation axis; such a choice ensures that, neglecting the effects of rotational distortion, each grid point encompasses an approximately equal surface area. Furthermore, there are $N_{eq}/4$ such coaxial rings between equator and pole, leading to a stellar grid approximately N_{eq}^2/π points in size, although storage requirements for the grid are only of order $N_{eq}/4$ due to the rotational and reflectional symmetry of the star. Throughout this paper, N_{eq} was taken to be 400, leading to a grid containing 51 030 points in total, of which (approximately) half are visible at any one time.

Once the radius at each grid point has been evaluated, the effective gravitational potential Φ defines the local (scalar) gravity

$$g_\theta = |\nabla\Phi|, \tag{33}$$

and the local surface normal,

$$\hat{\boldsymbol{n}}_\theta = \nabla\Phi/g_\theta, \tag{34}$$

with the usual convention that the surface normal points outwards from the surface. Gravity darkening (von Zeipel 1924; Cranmer & Collins 1993) then leads to a photospheric temperature at each grid point given by

$$T_\theta = T_p\left(\frac{g_\theta}{g_p}\right)^\beta, \tag{35}$$

where the value of the exponent β depends on whether the photosphere is radiative or convective; a value of 0.25, appropriate for early-type stars, is used throughout this paper (von Zeipel 1924). The effects of gravity darkening are to emphasize the formation of some species at the poles, and other species at the equator; this has important implications for the relative strengths of line-profile variability in different species if the pulsation is confined to the equatorial regions (Walker 1991; Reid et al. 1993; Howarth & Reid 1993). A similar effect arises from the dependence of line profiles on g_θ.

The surface area associated with each grid point is given by the modulus of the vector $\mathrm{d}\boldsymbol{A}$,

$$\mathrm{d}\boldsymbol{A} = R^2 \sin\theta\, \mathrm{d}\theta\, \mathrm{d}\phi \left(\hat{\boldsymbol{r}} - \frac{1}{R}\frac{\mathrm{d}R}{\mathrm{d}\theta}\hat{\boldsymbol{\theta}}\right), \tag{36}$$

where the symbols have their usual meanings; $\mathrm{d}\boldsymbol{A}$ is, by definition, parallel to $\hat{\boldsymbol{n}}_\theta$.

It is again to be emphasized that the use of a 'full' stellar grid covering the complete surface of the star allows the effects of rotational distortion to be handled elegantly and efficiently. As was discussed in Section 2, the effects of the rotational deformation on the gross characteristics of pulsation modes are generally small, and may be neglected; however, for rapidly rotating stars such as HD 93521 (Howarth & Reid 1993), a rotationally modified stellar grid is *essential* not only for reproduction of gravity-darkened line profiles, but also for the study of the relative strengths of line-profile variability. Furthermore, it is possible to use the full grid to 'image' the surface of the star from any position, providing strong links with the star as a physical entity.

4.2 Perturbing the grid

4.2.1 Velocity fields

The pulsational velocity fields defined in Section 3.3 are added vectorially to the azimuthal rotational velocity $\boldsymbol{\Omega} \times \boldsymbol{R}$ to give the full perturbed velocity field of each surface element. The value used for K in equation (6) is that dictated by the outer mechanical boundary condition, namely

$$K = \frac{1}{\bar{\omega}^2} \equiv \frac{GM}{\omega^2 R^3}. \tag{37}$$

Since this expression is derived under the assumption of spherical geometry, it is not immediately clear at what value of θ to take $R(\theta)$; throughout this paper, R is taken to equal R_p in the calculation of K. The use in models of theoretically correct values for K is in contrast with other authors (Aerts & Waelkens 1993; Howarth & Reid 1993) who choose K in an arbitrary way to differentiate between g-modes and p-modes. The theoretical value of K is used to maintain the self-consistency of the model and ensure that the inter-dependence of various pulsation phenomena is preserved; it is, however, possible to override this theoretical value if required in phenomenological applications.

The non-spherical nature of the stellar grid leads to non-radial surface normals. The question arises as to whether so-called 'radial' velocity fields should be directed along the local radial vector or the local surface normal vector. From a physical standpoint, the local surface normal would seem to be the more natural choice, since it defines the direction of the effective gravitational field and hence the direction of atmospheric stratification. However, it should be noted that applying the formalism of LS to a non-spherical star is a hybrid approach, since LS neglect the effect of the rotational deformation on the pulsation fields. Lee & Baraffe (1995) do consider such effects, but their theory is inherently far more computationally expensive than that of LS due to the inability to apply a diagonalization technique to their coupled pulsation equations. BRUCE is able to apply the 'radial' velocity fields either along the local surface normal (with the 'horizontal' velocity fields in corresponding perpendicular directions) or along the local radial vector; the latter is the default.

To allow consideration of the mechanisms behind different line-profile variability phenomena, BRUCE is designed to allow as an option the use of single spherical harmonics Y_l^m instead of the full rotational basis defined in Section 3.3; furthermore, horizontal velocity fields may be suppressed to allow the study of the effects of radial velocity fields alone.

4.2.2 *Temperature perturbations*

Dziembowski (1977) and Buta & Smith (1979) independently considered the effect of pulsational compression and rarefaction on the local photospheric temperature, for a star undergoing NRP within the Cowling approximation. Buta & Smith (1979) demonstrated that the magnitude of local temperature variations, for adiabatic pulsations, is given by

$$\frac{\delta T}{T} = \left(\frac{\Gamma_2 - 1}{\Gamma_2}\right)[K\Lambda(l) - 4 - 1/K]\frac{\delta R}{R}, \tag{38}$$

where the adiabatic exponent Γ_2 is taken to be 5/3 throughout this paper. LS generalized this expression to encompass non-adiabatic effects by assuming that the amplitude of the intensity variations introduced by the variations in T was proportional to the pulsational velocity, with the inclusion of some phase-shift factor ψ, so that the surface intensity I_0 is given by

$$I_0 = I_{00}\left\{1 + f\Re\left[|\lambda_{l,m}\rangle e^{i(\omega t+\psi)}\right]\right\}, \tag{39}$$

where I_{00} is a constant and f governs the amplitude of the intensity changes caused by the temperature perturbations (LS). For an adiabatic case, $\psi = \pm\pi/2$ and f is found from equation (38). BRUCE assumes a temperature-dependence given by equation (38) by default, but additional amplitude scalings and phase shifts may be introduced to account for non-adiabaticity. It should be noted that a significant effect of non-adiabaticity is that the symmetry of variability across a line profile, present in the adiabatic case, is removed, and different degrees of variability will be seen at opposing wings of a line profile.

LS comment that their equations [A10], which govern the radial eigenfunctions of the star under the traditional approximation, are identical to the equations governing NRP in non-rotating stars, apart from the replacement of a term $\Lambda(l)$ by $\lambda_{l,m}$. It is therefore plausible that any modification of equation (38) to take into account the effects of rotation should include a similar replacement. However, such a modification may lead to difficulties, since there exist values of ν at which $\lambda_{l,m}^{-1} = 0$. Because such points represent asymptotic lines in the $\Omega - \omega$ plane (Lee & Saio 1986), the situation where $\lambda_{l,m}^{-1} = 0$ never occurs in a model that uses consistent values for ω. Since BRUCE takes ω to be a free parameter, the replacement of $\Lambda(l)$ with a rotationally correct value is deferred until BRUCE is fully integrated with a model for the stellar interior.

4.2.3 *Geometric perturbations*

Buta & Smith (1979) also considered the geometrical effects of pulsation on the apparent brightness of a surface element. The geometrical effects are essentially twofold: the first is a variation in the area of a surface element, leading to a change in the net radiation flux through that element, whilst the second is a variation in the surface normal of the element, which when combined with a suitable limb-darkening law will lead to changes in the observed brightness. These two effects can be considered together by evaluating the perturbed surface area vector $d\boldsymbol{A}'$. Following Buta & Smith (1979), the perturbed position vector of a grid point $\boldsymbol{R}'$ is given by

$$\boldsymbol{R}' = (R + \delta R)\hat{\boldsymbol{r}}. \tag{40}$$

This expression neglects movements of the stellar surface due to horizontal velocity fields, but, since the equilibrium stellar configuration is static (apart from the uniform rotation), the local Lagrangian radius variation δR can also be considered an Eulerian quantity, and so equation (40) is correct to first order. The perturbed surface area vector is then

$$d\boldsymbol{A}' = \left(\frac{\partial \boldsymbol{R}'}{\partial \theta} \times \frac{\partial \boldsymbol{R}'}{\partial \phi}\right) d\theta d\phi, \tag{41}$$

where the derivatives are given by

$$\frac{\partial \boldsymbol{R}'}{\partial \theta} = R'\,\hat{\boldsymbol{\theta}} + \left(\frac{\partial R}{\partial \theta} + \frac{\partial \delta R}{\partial \theta}\right)\hat{\boldsymbol{r}} \tag{42}$$

and

$$\frac{\partial \boldsymbol{R}'}{\partial \phi} = R' \sin\theta\,\hat{\boldsymbol{\phi}} + \frac{\partial \delta R}{\partial \phi}\hat{\boldsymbol{r}}, \tag{43}$$

and $R' \equiv |\boldsymbol{R}'|$. It is important to note that equation (42) differs from the corresponding equation (3) of Buta & Smith (1979) due to the fact that the equilibrium stellar radius R is a function of θ on the rotationally distorted grid. Furthermore, these expressions assume that the direction of the 'radial' pulsation fields is indeed radial; as discussed in Section 4.2.1, this assumption may not be correct, but any errors introduced by it should be negligibly small. The projection of $\mathrm{d}\boldsymbol{A}'$ on to the line of sight then gives the perturbed values of the projected surface normal and the projected surface area.

It is interesting to observe that, if perturbations to the surface normal are neglected, a star may (theoretically) exhibit lpv due to surface velocity fields but show *no* ostensible photometric variability. Such a phenomenon may arise owing to cancellations between the temperature and surface-area variations. To investigate this, the intensity variations δI from a surface element may be expressed in the approximate form

$$\frac{\delta I}{I} = \chi_1 \frac{\delta R}{R} + \chi_2 \frac{\delta T}{T}, \tag{44}$$

where χ_1 and χ_2 are constants. For a radial pulsator, χ_1 is 2; in the non-radial case, its value depends on the pulsation mode under consideration, but is close to 2. In the case of a blackbody of temperature T, χ_2 is given by

$$\chi_2 = \frac{hc}{\lambda kT}\frac{\mathrm{e}^{hc/\lambda kT}}{\mathrm{e}^{hc/\lambda kT}-1}, \tag{45}$$

where the symbols have their usual meanings. In the case of adiabatic pulsation, equation (38) may be used to write equation (44) as

$$\frac{\delta I}{I} = \left\{1 + \frac{\chi_2}{\chi_1}\left(\frac{\Gamma_2 - 1}{\Gamma_2}\right)[K\Lambda(l) - 4 - 1/K]\right\}\frac{\delta R}{R}. \tag{46}$$

Setting $\delta I = 0$ as an appropriate condition for a lack of photometric variability, and assuming that $\delta R \neq 0$, leads to a quadratic equation in K, with roots K_0 given by

$$K_0 = \frac{-\Gamma' \pm \sqrt{\Gamma'^2 + 4\Lambda(l)}}{2\Lambda(l)}, \tag{47}$$

where Γ' is given by

$$\Gamma' = \frac{\chi_1 \Gamma_2}{\chi_2(\Gamma_2 - 1)} - 4. \tag{48}$$

Thus, for stars pulsating with K near the 'critical' value K_0, one would expect to observe little or no photometric (continuum) variability. It should be emphasized that equation (47) is an approximation – photometric variability may not totally vanish for *any* value of K, due to the non-constancy of χ_1 and χ_2 in equation (44). More significantly, the neglected surface-normal perturbations are not *phase-coherent* with the temperature and surface-area perturbations; that is, the former are not exactly in phase or anti-phase with the latter. As a consequence, the surface-normal perturbations cannot cancel with the temperature or surface-area perturbations through the interference mechanism just demonstrated. Whether this absence of cancellation is enough to obscure the 'photometric minimum' described herein is considered in Section 6.3.

5 LINE-PROFILE SYNTHESIS

5.1 Theoretical background

Once the stellar grid has been perturbed using the velocity fields and other mechanisms discussed in the preceding section, individual emergent spectra must be calculated for each grid point. These individual spectra are co-added to produce the resultant spectrum of the entire model star; generation of a time-resolved sequence of such spectra allows a confrontation between theoretical models and observed line-profile variability thought to arise from NRP. In the past, most authors (Pesnell 1985; Kambe & Osaki 1988; Lee & Saio 1990; Lee, Jeffery & Saio 1992; Aerts & Waelkens 1993; Schrijvers et al. 1996) have modelled intrinsic spectral line profiles with Gaussians. Since the majority of early-type stars exhibit lines with a rotational width far in excess of the intrinsic width, the use of Gaussians would *appear* to be adequate for the modelling of line-profile variability generated by photospheric velocity fields – Schrijvers et al. (1996) suggest that lpv resulting from velocity fields alone are insensitive to the choice of intrinsic profile. However, Smith (private communication) has stressed that, at least for large-l modes, the amplitude structure of lpv is strongly dependent on the interplay between the intrinsic line-profile morphology in velocity space and the rotational/pulsational velocity fields, and cannot be modelled properly without the use of 'correct' intrinsic profiles. Furthermore, a proper treatment must model the temperature-sensitivity of the intrinsic profiles accurately, not only to reproduce correctly the rotationally broadened spectral lines of the gravity-darkened star, but more importantly to calculate accurately the lpv resultant from local temperature changes. Some authors model the temperature sensitivity of lines using Gaussian intrinsic line profiles with variable equivalent widths; the equivalent width can be determined from a temperature-resolved grid (Lee et al. 1992), or from some assumed functional temperature dependence (Telting & Schrijvers 1996). Whilst such approaches represent an improvement on the constant equivalent width Gaussians used by other authors (Aerts

& Waelkens 1993), they only address one aspect (equivalent-width variation) of the temperature sensitivity of the intrinsic profiles, and will not reproduce the amplitude structure of lpv particularly accurately.

Of lesser importance, but still worthy of attention, is the manner in which the limb darkening is implemented. The majority of authors (Lee et al. 1992; Aerts & Waelkens 1993; Schrijvers et al. 1996) use a limb-darkening law for the specific intensity I at emergent angle θ in terms of the normally emergent intensity I_0 of the form

$$I(\theta) = \alpha_1 + I_0(\alpha_2 + \alpha_3 \cos\theta), \tag{49}$$

where α_1, α_2 and α_3 govern the specific behaviour of the limb darkening. Such treatments neglect the fact that the limb darkening is a function of both wavelength and photospheric temperature (especially across line profiles). Schrijvers et al. (1996) acknowledge the limitations of such simplifications, and point out that variations in the choice of limb-darkening parameters can lead to changes of up to 20 per cent in the observed line-profile variability.

Consideration of these issues and others, such as the requirement that the correspondence between the pulsational amplitude and the degree of line-profile variability be quantifiable, led to the implementation of the spectral synthesis within BRUCE using intrinsic line profiles calculated from a non-LTE model atmosphere code. A discussion of this implementation follows.

5.2 Implementation

At each grid point, the inclination of the (suitably perturbed) surface normal to the line of sight is calculated. This inclination, along with the gravity-darkened and pulsationally modified photospheric temperature, and the local effective gravity, is used by a set of routines (Smith & Howarth 1994, section 4) to interpolate in a grid of pre-calculated non-LTE synthetic spectra. This approach represents a significant departure from the use of Gaussians, since within the context of the atmospheric models all lines considered have correct temperature sensitivities and intrinsic profiles, and exhibit the correct limb-darkening behaviour. The use of these line profiles not only allows proper consideration of the temperature perturbations; but also, when coupled with gravity darkening, rotationally broadened profiles for the complete model star can be constructed which reproduce observations well. It cannot be emphasized too strongly that correct treatment of the intrinsic profile morphology – and the *behaviour* of this morphology with varying temperature and varying limb parameter – is *essential* for the calculation of realistic lpv; the use of the non-LTE spectral grid in BRUCE ensures that intrinsic profiles have both the required morphology *and* the required behaviour. It is interesting to note that, in their seminal paper, Vogt & Penrod (1983) used a similar approach to model the intrinsic line profiles; however, they interpolated their spectra in one dimension between two temperature/gravity points, rather than performing a two-dimensional interpolation in a fine temperature–gravity mesh. Furthermore, the spectra used by them were calculated from LTE, rather than non-LTE, model atmospheres.

Once the (suitably Doppler-shifted) emergent spectra for each grid point have been interpolated, they are weighted with the projected surface area of the grid points and co-added to form a resultant spectrum for the whole star. By translating pulsation patterns around the surface of the stellar grid to simulate both stellar rotation and the passage of time, BRUCE is able to construct time-resolved sets of spectra for the model pulsating star, which may then be compared with observations to deduce the fundamental pulsation parameters. Some preliminary results from BRUCE are presented in the next section, illustrating the importance of various pulsational phenomena and implementation issues as discussed previously.

6 RESULTS

To provide an illustration of some of the calculations performed using BRUCE, results are presented from the modelling of a star the parameters of which, given in Table 1, were chosen to correspond approximately to those of ζ Oph. The table specifies both the free parameters, which uniquely determine the star being modelled, and the derived parameters, which are calculated using the appropriate relations from the free parameters. A focus on three specific areas of general pulsation phenomena follows; these (preliminary) investigations are in no way exhaustive, and serve merely to illustrate some of the applications of BRUCE. It is anticipated that the bulk of the exploration of parameter space using BRUCE will appear in subsequent papers.

Table 1. Free and derived parameters for the modelled ζ Oph-type star.

Free		Derived	
Polar gravity, g_p	4.00 dex	Equatorial gravity, g_{eq}	3.73 dex
Polar temperature, T_p	38000 K	Equatorial temperature, T_{eq}	32500 K
Polar radius, R_p	9.0 $R_\odot$	Equatorial radius, R_{eq}	10.3 $R_\odot$
Equatorial velocity, V_{eq}	400 kms^{-1}	Angular rotation frequency, Ω	5.57×10^{-5} s^{-1}
Inclination, i	60°	Stellar mass, M	29.6 $M_\odot$

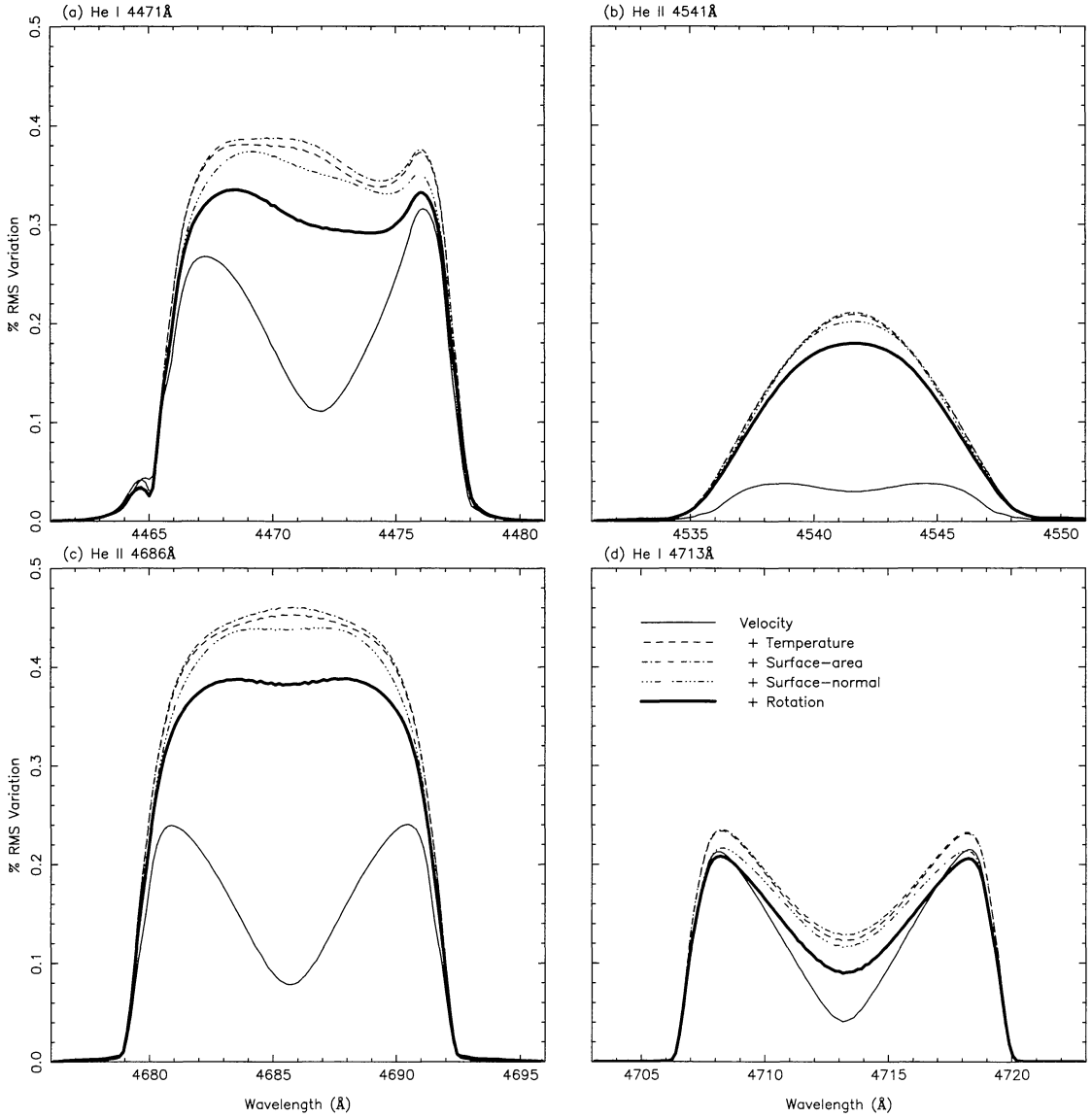

Figure 4. Rms variability spectra (as a percentage of the continuum) for an $l = 8$, $m = -8$ pulsation mode in the (a) He I 4471-Å, (b) He II 4541-Å, (c) He II 4686-Å and (d) He I 4713-Å lines. The pulsations modelled included (cumulatively) velocity fields (thin solid), temperature variations (dashed), area variations (dot-dash), surface-normal variations (dash-dot-dot-dot-dash) and rotationally modified normal modes (thick solid). The maximum velocity amplitude in all cases was normalized to 40 km s^{-1}.

6.1 Relative importance of the perturbations

To investigate the relative importance of the perturbations discussed in Section 4.2, a number of synthetic spectra were calculated for a star pulsating in an $l = -m = 8$ prograde sectoral mode with a corotating pulsation period of 12.8 h (i.e. g-mode domain), leading to a period in an inertial frame of 3.0 h. The rotation parameter ν was calculated to be 0.77, so the effects of rotation were expected to be small but non-negligible. The pulsation amplitude was chosen so that the maximum pulsation velocity $|v_{\rm osc}|$ on the stellar surface was always 40 km s^{-1}. Time-series of 24 spectra, covering exactly one pulsation period, were calculated with the inclusion or omission of some of the perturbations discussed in Section 4.2. The results of these time series are displayed in Fig. 4; for each of the four spectral lines modelled, the time-averaged rms variation of the rectified individual spectra from the rectified mean spectrum is plotted as a function of the wavelength, in percentage units of the continuum. The thin solid line shows these rms variability spectra (RVS) for a model including solely velocity fields proportional to a single spherical harmonic. The dashed line represents the same model with the addition of temperature perturbations following the adiabatic relation described in Section 4.2.2; the dot-dashed and dash-dot-dot-dot-dashed lines represent the *further* inclusion of the perturbed surface areas and perturbed surface normals respectively (Section 4.2.3). Finally, the thick solid line shows the effect of using the rotationally modified pulsation modes discussed previously instead of terms proportional to single spherical harmonics.

Examination of Fig. 4 leads to a number of conclusions about the relative importance of the various perturbations implemented in BRUCE. First, it is evident that the inclusion of temperature perturbations has a *dramatic* effect on the RVS. The temperature variations serve to increase

the line-profile variability primarily in the line centres, although some increase in variability is also observed at the line wings. LS suggested that the inclusion of temperature perturbations could partially resolve a current modelling problem, namely that the g-mode pulsations simulated solely with velocity fields failed to produce the observed amount of line-profile variability in the line centres. The results presented here would seem to support that argument. Note that the adiabaticity of the temperature perturbations manifests itself in the symmetry of the RVS about the line centres; the asymmetry in the He I 4471-Å line arises from contamination by a quasi-forbidden He I component at 4470 Å.

Inclusion of the geometric perturbations has relatively little effect on the line-profile variability. Although in some of the lines, especially He I 4471 Å, inclusion of the geometric perturbations leads to a (theoretically) noticeable change in the RVS, this change has no distinguishing signature and probably falls below the current threshold of observational detectability. The use of rotationally modified pulsation modes has a more significant effect on the RVS; in general, the degree of variability is decreased, with the reduction strongest in the line centres. This reduction arises from two sources. First, the equatorial compression of pulsation modes, discussed in Section 3.3, means that less of the stellar surface shows pulsation activity of a detectable amplitude, and so the observed variability will decrease, especially in the pole-formed line centres. Secondly, the domination of the rotationally modified pulsation modes by toroidal velocity fields means that, for the velocity-amplitude normalization described above, the strength of the radial velocity fields will be smaller in a rotating star than in a non-rotating star. Since these radial velocity fields contribute to line-profile variability primarily in the line centres, there will be a corresponding decrease in the observed line centre variability.

6.2 Gravity darkening and equatorial compression

Observations of lpv rapidly rotating in early-type stars show that line-profile variability appears to be weakest in lines of species of highest ionization potential (Walker 1991; Reid et al. 1993). It has been suggested (Walker 1991; Reid et al. 1993; Howarth & Reid 1993) that, since species of highest ionization are formed towards the (hotter) pole in a gravity-darkened star, this phenomenon arises from pulsation modes the activity of which is concentrated around the equator, namely sectoral modes and modes of small $(l - |m|)$. This argument has been used (Walker 1991) to justify the use of mainly sectoral-mode pulsations in modelling NRP.

However, as was demonstrated in Section 3.3, rotation acts to confine pulsation activity towards the stellar equator; furthermore, this confinement is largest at a given rotation rate for modes with *large* $(l - |m|)$. Thus one would expect to observe this differential variability strength phenomenon not only for sectoral modes, but also for all varieties of tesseral modes. To investigate whether indeed this is the case, the spectra of an extremely rapidly rotating $l = 8$, $m = -3$ pulsator were calculated, with velocity fields proportional to both the rotationally modified basis states $|\lambda_{l,m}\rangle$, and single spherical harmonics Y_l^m. The stellar parameters used were those for the ζ Oph-type star given in Table 1, except that the equatorial rotation velocity $V_{\rm eq}$ was raised to 500 km s^{-1} to simulate very rapid rotation. In this case, the equatorial temperature $T_{\rm eq}$ was pushed down to 28 600 K, so the star exhibited quite strong gravity darkening. Furthermore, the corotating pulsation period ω was chosen to give a rotation parameter ν of 3.0, so the effects of rotation on the pulsation mode (when included) were quite severe (see Fig. 3). Perturbations to the temperature, surface area and surface normal were omitted to allow concentration on the effects of velocity fields alone. Fig. 5 shows the RVS in the He II line at 4686 Å and the He I line at 4713 Å for (a) the model using velocity fields proportional to a single spherical harmonic, and (b) the model using velocity fields proportional to the rotationally modified basis state $|\lambda_{l,m}\rangle$; in all cases, the maximum velocity amplitude $|v_{\rm osc}|$ on the stellar surface was normalized to 40 km s^{-1}. Under each spectrum is a map of the radial pulsation velocity across the stellar disc; map (b) demonstrates the high degree of equatorial confinement which the rotation introduces. The rotational distortion of the equilibrium stellar figure has been suppressed in these maps. Note that the large amount of structure in the RVS is a consequence of the mode being modelled, and not due to temporal or spatial under-sampling.

It is apparent that the effect of using the equatorially confined basis states $|\lambda_{l,m}\rangle$ is to decrease the degree of activity in the line centres. The reasons for this decrease were discussed in the preceding section, and are not relevant here. Of greater importance, though, is the fact that there is no apparent decrease in the *maximum* variability of the equatorially formed He I 4713-Å line, but a halving in the variability of the pole-formed He II 4686-Å line; it appears that the phenomenon discussed by Walker (1991) is not just restricted to sectoral modes, but may manifest itself in tesseral modes with higher values of $(l - |m|)$. This phenomenon can no longer be used to justify the exclusive use of sectoral modes when modelling NRP, and it is thus important to include full consideration of tesseral, zonal and quasi-toroidal modes in any treatment.

6.3 Continuum variations

It is possible, as was demonstrated in Section 4.2.3, that a star *might* exhibit line-profile variations but show little associated photometric variability. To test this hypothesis, time-series continuum spectra were generated for the ζ Oph-type star discussed previously; the star was taken to be pulsating in an $l = 2, m = -2$ sectoral mode. Conventional wisdom (e.g. Buta & Smith 1979) is that a star pulsating in such a mode would be expected to exhibit photometric variability above the detectable threshold for realistic pulsation amplitudes; the pulsation amplitude was normalized so that the maximum pulsation velocity $|v_{\rm osc}|$ on the stellar surface was 40 km s^{-1}. The rms variability of the *unrectified* spectra at the 5100-Å continuum wavelength (chosen as well-separated from hydrogen and helium lines) was calculated as a function of the parameter K; the pulsation frequencies were chosen to be consistent with K via equation (37). Fig. 6 shows the rms variability in magnitudes

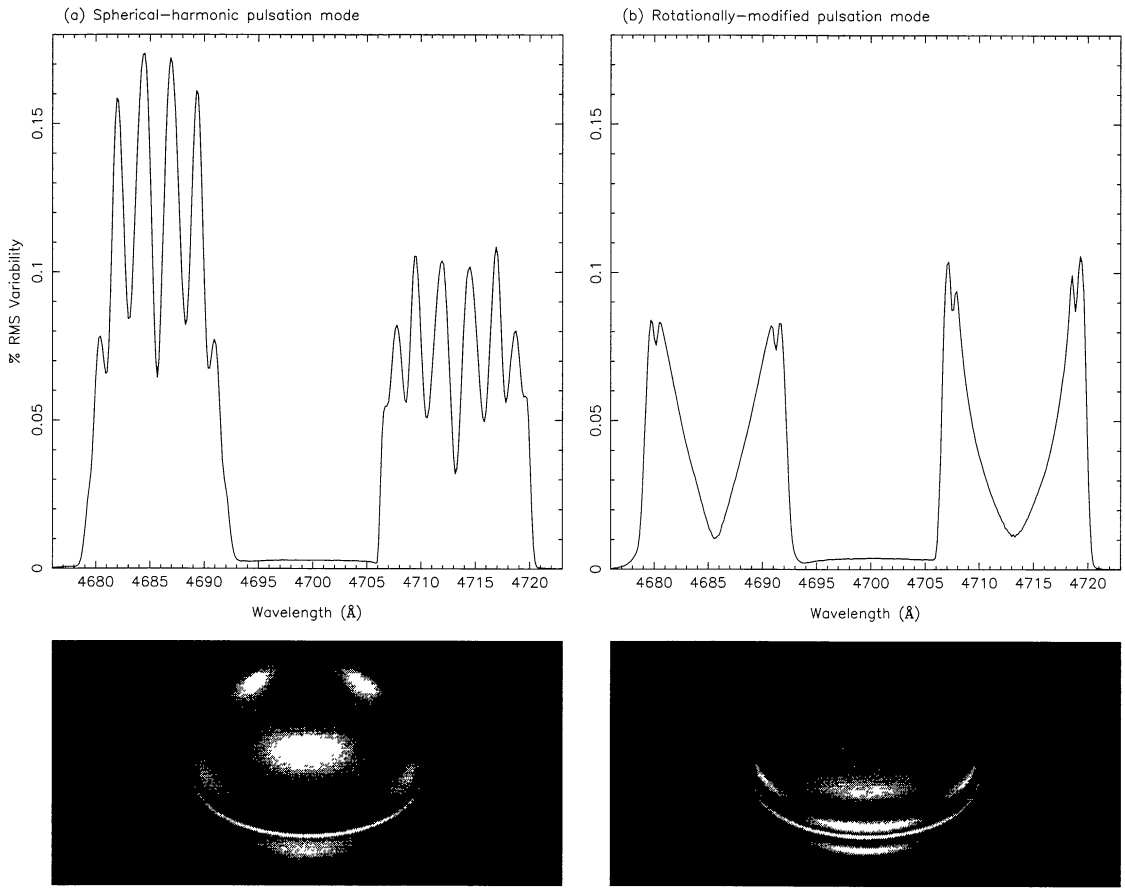

Figure 5. Rms variability spectra covering the He II 4686-Å and He I 4713-Å lines for an $l = 8$, $m = -3$ pulsation mode proportional to (a) a single spherical harmonic and (b) the appropriate rotationally modified basis state $|\lambda_{l,j,m}\rangle$. The maximum velocity amplitude in both cases was normalized to 40 km s^{-1}. Underneath each spectrum is an velocity map (neglecting rotation) of the stellar pulsation as it would appear to an observer; the ring around the star marks the equator.

for (a) a model containing solely temperature perturbations, (b) a model containing solely surface-area perturbations, (c) a model containing both of these perturbations, and (d) a model containing all temperature, surface-area and surface-normal perturbations. In all cases, pulsation modes proportional to single spherical harmonics were used, since the effect of rotation on the pulsation modes was not considered relevant in this particular study.

Of particular note in all four panels is the discontinuity in the gradient of the rms variability at $K \sim 0.5$. This discontinuity is a consequence of the method of normalization chosen to maintain the *maximum* pulsation velocity $|v_{\rm osc}|$ at 40 km s^{-1}. This normalization is accomplished by dividing the amplitude A in equation (19) by some function $A^0_{l,j,m}(V_{\rm max}, K)$, which depends upon both K and the maximum pulsation velocity $V_{\rm max}$, here taken to be 40 km s^{-1}. The function $A^0_{l,j,m}(V_{\rm max}, K)$ is constant when the velocity fields are dominated by radial terms, and proportional to K when the velocity fields are dominated by horizontal terms (e.g. Kambe & Osaki 1988); at the interface between these two domains, which occurs here at $K \sim 0.5$, $A^0_{l,j,m}(V_{\rm max}, K)$ is continuous but its *gradient* shows a discontinuity. This normalization feature leads to the gradient discontinuity in the rms variability at $K \sim 0.5$.

Panel (a) shows a zero in the rms variability at $K \sim 0.85$; this occurs at the point where the term in brackets in equation (38) is identically zero. This zero will manifest itself in models considering only temperature perturbations, and will not be observed in any real star. For $K \lesssim 0.85$, the temperature perturbations are in anti-phase with the surface-area perturbations illustrated in panel (b). Taking approximate values of 2 and 1.5 for χ_1 and χ_2 respectively in equation (48), which are appropriate for a blackbody at 32 000 K and 5100 Å, the value K_0 at which one expects the temperature and surface-area perturbations to cancel one another is found using equation (46) to be approximately 0.47; this corresponds to the minimum in the rms variability illustrated in panel (c), and demonstrates that the interference between the temperature and surface-area perturbations discussed in Section 4.2.3 does indeed occur.

Inclusion of the surface-normal perturbations serves to obscure this photometric minimum totally, as is evident in diagram (d). As discussed in Section 4.2.3, the surface-normal perturbations do not exhibit an interference phenomenon with other perturbations due to a lack of phase coherence; hence, with all perturbations properly included, one would *not* expect to observe a photometric minimum. It is thus *vital* to include surface-normal perturbations if either temperature or surface-area perturbations are included in a photometric (continuum) study of the stellar pulsation; otherwise, calculations of photometric variability may be highly inaccurate.

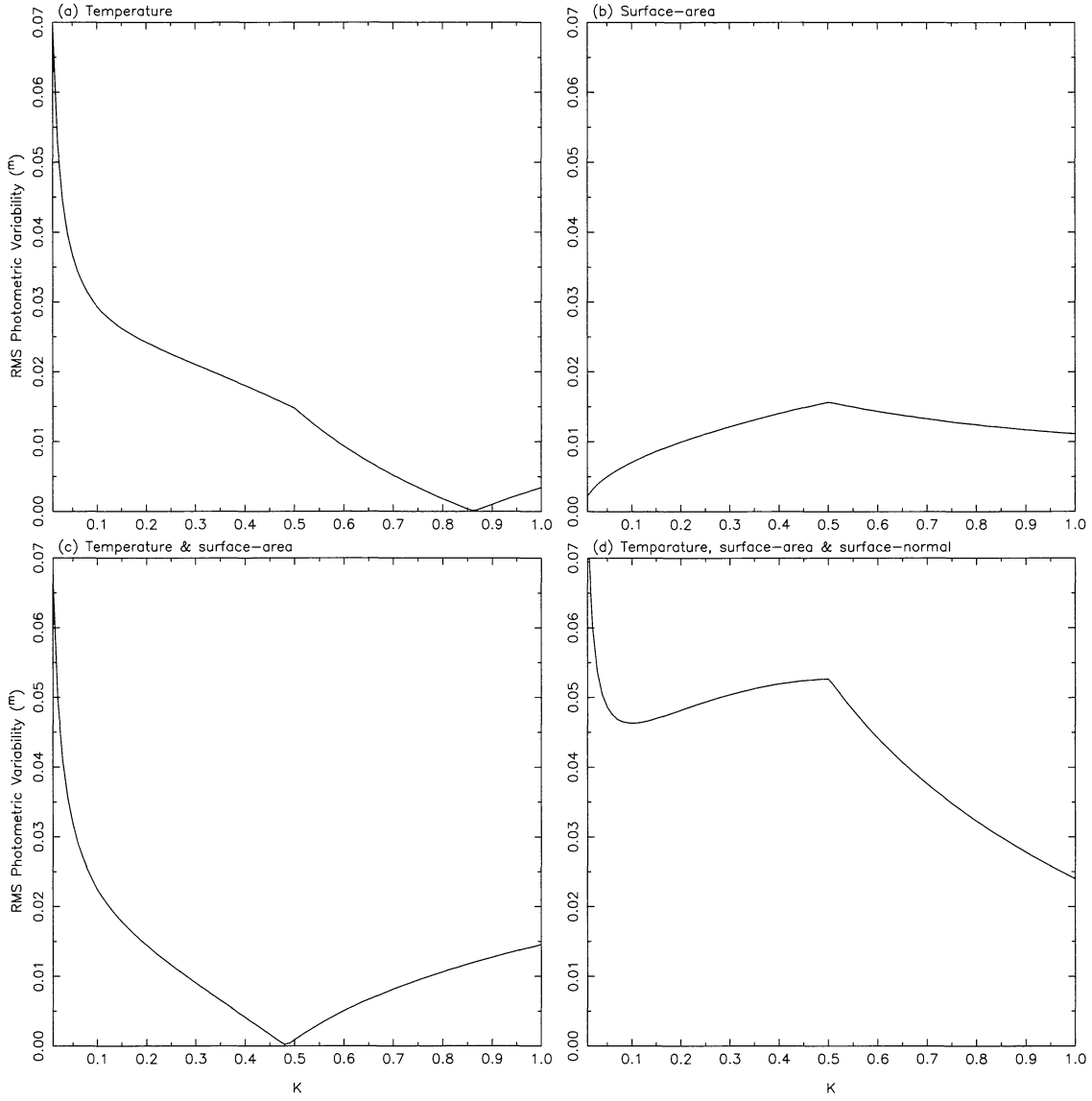

Figure 6. Rms variability at 5100 Å for an $l = -m = 2$ pulsation mode as a function of K, with the inclusion of (a) temperature perturbations, (b) surface-area perturbations, (c) both of these and (d) temperature, surface-area *and* surface-normal perturbations. The maximum velocity amplitude in all cases was normalized to 40 km s^{-1}; this normalization leads to the gradient discontinuities apparent at $K \sim 0.5$.

7 SUMMARY

A new computer code, BRUCE, has been presented which models pulsation in rapidly rotating early-type stars. The code includes consideration of surface velocity fields and local-temperature, surface-normal and surface-area variations. Modes of pulsation proportional to linear sums of spherical harmonics are included, to account for the effects of the Coriolis force on the pulsation. The spectral lines generated by the code are based on intrinsic line profiles calculated from non-LTE model atmospheres.

It is found that the rotation compresses pulsational activity towards the equator, and treatment of this phenomenon, when coupled with a gravity-darkened stellar grid, leads to a significant change in the calculated variability strengths of spectral lines of high- and low-ionization states. Inclusion of temperature perturbations in the model leads to significant modifications to the degree of line-profile variability observed. Perturbations to the surface area and surface normals are shown to have only a small effect on the line-profile variability, most likely below the detectable threshold; however, it is demonstrated that a proper consideration of the interplay between the surface-area, surface-normal and temperature perturbations is vital for correct modelling of the (detectable) photometric variability.

Although BRUCE represents an elaboration on other previous spectral-synthesis NRP models, the prospect of probing early-type stars using asteroseismological techniques of detail comparable to current helioseismological methods requires modelling and observations of greater sophistication than currently available. Of particular importance are better treatments of the effects of rotation, both on the stellar structures and on the pulsation modes, and the development of fully non-linear non-adiabatic models. However, it is hoped that, with BRUCE, initial *quantitative* (albeit crude) rather than qualitative investigations of NRP may be embarked upon.

ACKNOWLEDGMENTS

I am indebted to Keith Smith for the use of his grid of synthetic spectra. Thanks also go to Ian Howarth and Andy Reid for many interesting and informative discussions, and to Myron Smith for useful discussions and comments on a draft of this manuscript. This research is supported by a PPARC studentship.

REFERENCES

Abramowitz M., Stegun I., 1964, Applied Mathematics Series 55, Handbook of Mathematical Functions. National Bureau of Standards, USA
Aerts C., Waelkens C., 1993, A&A, 273, 135
Aerts C., Waelkens C., 1995, A&A, 293, 978
Arfken G., 1970, Mathematical Methods for Physicists. Academic Press, London
Berthomieu G., Gonczi G., Graff P., Provost J., Rocca A., 1978, A&A, 70, 597
Buta R., Smith M. A., 1979, ApJ, 232, 213
Clement M. J., 1981, ApJ, 249, 746
Collins G. W., Harrington J. P., 1966, ApJ, 146, 152
Cowling T. G., 1941, MNRAS, 101, 367
Cranmer S. R., Collins G. W., 1993, ApJ, 412, 720
Dziembowski W., 1977, Acta Astron., 27, 95
Fullerton A. W., Gies D. R., Bolton C. T., 1996, ApJS, 103, 475
Howarth I. D., Reid A. H. N., 1993, A&A, 279, 148
Kambe E., Osaki Y., 1988, PASJ, 40, 313
Kambe E., Ando H., Hirata R., 1990, PASJ, 42, 687
Kurtz D. W., 1982, MNRAS, 200, 907
Ledoux P., 1951, ApJ, 114, 373
Lee U., Baraffe I., 1995, A&A, 301, 419
Lee U., Saio H., 1986, MNRAS, 221, 365
Lee U., Saio H., 1987, MNRAS, 224, 513
Lee U., Saio H., 1989, MNRAS, 237, 875
Lee U., Saio H., 1990, ApJ, 349, 570 (LS)
Lee U., Jeffery C. S., Saio H., 1992, ApJ, 254, 185
Leighton R. B., Noyes R. W., Simon G. W., 1962, ApJ, 135, 474
Martens L., Smeyers P., 1982, A&A, 106, 317
Osaki Y., 1971, PASJ, 23, 485
Papaloizou J., Pringle J. E., 1978, MNRAS, 182, 423
Parlett B., 1980, The Symmetric Eigenvalue Problem. Prentice-Hall, Englewood Cliffs
Pesnell W. D., 1985, ApJ, 292, 238
Press W., Teukolsky S., Vetterling W., Flannery B., 1992, Numerical Recipies in Fortran. Cambridge Univ. Press, Cambridge
Reid A. H. N., Howarth I. D., 1996, A&A, 311, 616
Reid A. H. N. et al., 1993, ApJ, 417, 320
Saio H., 1981, ApJ, 244, 299
Saio H., 1982, ApJ, 256, 717
Schrijvers C., Telting J. H., Aerts C., Ruymaekers E., Henrichs H. F., 1996, A&A, in press
Smith K. C., Howarth I. D., 1994, A&A, 290, 868
Smith M. A., 1977, ApJ, 215, 574
Smith M. A., Karp A. H., 1976, in Cox A. N., Deupree R. G., eds, Proc. Solar and Stellar Pulsation Conf. Los Alamos Publ., p. 289
Tassoul M., 1980, ApJS, 43, 469
Telting J. H., Schrijvers C., 1996, A&A, in press
Thomson W., 1863, Phil. Trans. R. Soc. London, 153, 612
Tinkham M., 1964, Group Theory and Quantum Mechanics. McGraw-Hill, USA
Unno W., Osaki Y., Ando H., Saio H., Shibahashi H., 1989, Nonradial Oscillations of Stars. University of Tokyo Press, Tokyo
Vogt S. S., Penrod G. D., 1983, ApJ, 275, 661
von Zeipel H., 1924, MNRAS, 84, 665
Walker G. A. H., 1991, in Baade D., ed., ESO Workshop 36, Rapid Variability of OB Stars. ESO, Garching, p. 27
Walker G. A. H., Yang, S., Fahlman G. G., 1979, ApJ, 233, 199

APPENDIX A: THE COMPONENTS OF $\aleph$

Lee & Saio (1987) gave expressions for the components of the coupling matrix $\aleph$ for even modes. To find the corresponding expressions for odd modes, a series of algebraic manipulations on the constituent matrices of $\aleph$ must be performed. To simplify these manipulations, the following easily proven identities are introduced.

Identity 1. The inverse of any diagonal matrix $\mathbf{D}$ is diagonal, with non-zero components given by

$$(\mathbf{D}^{-1})_{j,j} = (\mathbf{D})_{j,j}^{-1}. \tag{A1}$$

Identity 2. The product of any matrix $\mathbf{M}$ with a diagonal matrix $\mathbf{D}$ has components given by

$$(\mathbf{MD})_{i,j} = (\mathbf{M})_{i,j}(\mathbf{D})_{j,j}. \tag{A2}$$

Identity 3. The product of a diagonal matrix $\mathbf{D}$ with any matrix M has components given by

$$(\mathbf{DM})_{i,j} = (\mathbf{D})_{i,i}(\mathbf{M})_{i,j}. \tag{A3}$$

Identity 4. The product of any upper bidiagonal matrix $\mathbf{M}^b$ with any lower bidiagonal matrix $\mathbf{M}_b$ is tridiagonal with non-zero components given by

$$(\mathbf{M}^b\mathbf{M}_b)_{j,j} = (\mathbf{M}^b)_{j,j}(\mathbf{M}_b)_{j,j} + (\mathbf{M}^b)_{j,j+1}(\mathbf{M}_b)_{j+1,j}, \tag{A4}$$

$$(\mathbf{M}^b\mathbf{M}_b)_{j+1,j} = (\mathbf{M}^b)_{j+1,j+1}(\mathbf{M}_b)_{j+1,j}, \tag{A5}$$

$$(\mathbf{M}^b\mathbf{M}_b)_{j,j+1} = (\mathbf{M}^b)_{j,j+1}(\mathbf{M}_b)_{j+1,j+1}. \tag{A6}$$

With these identities, the evaluation of the components of $\aleph$ follows from the definitions of Lee & Saio (1987). For odd modes, $\aleph$ is given by

$$\aleph = (\mathbf{L}_0 - \mathbf{M}_0\mathbf{L}_1^{-1}\mathbf{M}_1)\Lambda^{-1}, \tag{A7}$$

where the matrices $\mathbf{L}_0$, $\mathbf{M}_0$, $\mathbf{L}_1$, $\mathbf{M}_1$ and Λ are defined by Lee & Saio (1987). To evaluate $\aleph$, an expression for the components of $\mathbf{L}_1^{-1}\mathbf{M}_1$ is required. $\mathbf{L}_1$ is a symmetric matrix, and therefore so is $\mathbf{L}_1^{-1}$. Thus, using the identities,

$$(\mathbf{L}_1^{-1}\mathbf{M}_1)_{j,i} = (\mathbf{L}_1)^{-1}_{j,j}(\mathbf{M}_1)_{j,i}. \tag{A8}$$

Since $\mathbf{M}_1$ is a $\mathbf{M}_b$-type matrix, the only non-zero components of $\mathbf{L}_1^{-1}\mathbf{M}_1$, which is also a $\mathbf{M}_b$-type matrix, will then be given by

$$(\mathbf{L}_1^{-1}\mathbf{M}_1)_{j,j} = (\mathbf{L}_1)^{-1}_{j,j}(\mathbf{M}_1)_{j,j}, \tag{A9}$$

$$(\mathbf{L}_1^{-1}\mathbf{M}_1)_{j+1,j} = (\mathbf{L}_1)^{-1}_{j+1,j+1}(\mathbf{M}_1)_{j+1,j}. \tag{A10}$$

Since $\mathbf{M}_0$ is an $\mathbf{M}^b$-type matrix, the tridiagonal matrix $\mathbf{A} = \mathbf{M}_0\mathbf{L}_1^{-1}\mathbf{M}_1$ is formed using the identity for the product of an $\mathbf{M}^b$-type matrix with an $\mathbf{M}_b$-type matrix. $\mathbf{A}$ has non-zero components given by

$$(\mathbf{A})_{j,j} = (\mathbf{M}_0)_{j,j}(\mathbf{L}_1)^{-1}_{j,j}(\mathbf{M}_1)_{j,j} + (\mathbf{M}_0)_{j,j+1}(\mathbf{L}_1)^{-1}_{j+1,j+1}(\mathbf{M}_1)_{j+1,j}, \tag{A11}$$

$$(\mathbf{A})_{j+1,j} = (\mathbf{M}_0)_{j+1,j+1}(\mathbf{L}_1)^{-1}_{j+1,j+1}(\mathbf{M}_1)_{j+1,j}, \tag{A12}$$

$$(\mathbf{A})_{j,j+1} = (\mathbf{M}_0)_{j,j+1}(\mathbf{L}_1)^{-1}_{j+1,j+1}(\mathbf{M}_1)_{j+1,j+1}. \tag{A13}$$

Inserting the expressions for the components of the matrices $\mathbf{M}_0$, $\mathbf{M}_1$ and $\mathbf{L}_1$ (Lee & Saio 1987) into equation (A11) leads to expressions for the non-zero components of $\mathbf{A}$:

$$(\mathbf{A})_{j,j} = \nu^2\left\{\frac{k_j(k_j+2)(J^m_{k_j+1})^2}{(k_j+1)^2[1-m\nu/\Lambda(n_j)]} + \frac{(k_j+1)(k_j+3)(J^m_{k_j+2})^2}{(k_j+2)^2[1-m\nu/\Lambda(n_j+2)]}\right\}, \tag{A14}$$

$$(\mathbf{A})_{j+1,j} = \nu^2\frac{\Lambda(k_j+1)J^m_{k_j+2}J^m_{k_j+3}}{\Lambda(k_j+2)[1-m\nu/\Lambda(n_j+2)]}, \tag{A15}$$

$$(\mathbf{A})_{j,j+1} = \nu^2\frac{\Lambda(k_j+3)J^m_{k_j+2}J^m_{k_j+3}}{\Lambda(k_j+2)[1-m\nu/\Lambda(n_j+2)]}, \tag{A16}$$

where the symbols J^m_l and k_j have the same meanings as those of Lee & Saio (1987). These expressions may be simplified if both k_j and n_j are written in terms of l_j; then the non-zero components of $\mathbf{A}$ become

$$(\mathbf{A})_{j,j} = \nu^2\left\{\frac{(l_j^2-1)(J^m_{l_j})^2}{l_j^2[1-m\nu/\Lambda(l_j-1)]} + \frac{l_j(l_j+2)(J^m_{l_j+1})^2}{(l_j+1)^2[1-m\nu/\Lambda(l_j+1)]}\right\}, \tag{A17}$$

$$(\mathbf{A})_{j+1,j} = \nu^2\frac{\Lambda(l_j)J^m_{l_j+1}J^m_{l_j+2}}{\Lambda(l_j+1)-m\nu}, \tag{A18}$$

$$(\mathbf{A})_{j,j+1} = \nu^2\frac{\Lambda(l_j+2)J^m_{l_j+1}J^m_{l_j+2}}{\Lambda(l_j+1)-m\nu}. \tag{A19}$$

Finally, since $\aleph$ is just the product of a tridiagonal matrix – formed from the difference of a diagonal matrix $\mathbf{L}_0$ and the tridiagonal matrix $\mathbf{A}$ – and a diagonal matrix Λ^{-1}, $\aleph$ itself is tridiagonal,with non-zero components given by

$$(\aleph)_{j,j} = [(\mathbf{L}_0)_{j,j} - (\mathbf{A})_{j,j}](\Lambda)^{-1}_{j,j}, \tag{A20}$$

$$(\aleph)_{j+1,j} = -(\mathbf{A})_{j+1,j}(\Lambda)^{-1}_{j,j}, \tag{A21}$$

$$(\aleph)_{j,j+1} = -(\mathbf{A})_{j,j+1}(\Lambda)^{-1}_{j+1,j+1}. \tag{A22}$$

Substituting in the components of $\mathbf{A}$, $\mathbf{L}_0$ and $\mathbf{\Lambda}$ gives these components as

$$(\aleph)_{j,j} = \left[1 - m\nu/\Lambda(l_j) - \nu^2 F(l_j)\right]/\Lambda(l_j), \tag{A23}$$

$$(\aleph)_{j+1,j} = (\aleph)_{j,j+1} = -\nu^2 J^m_{l_j+1} J^m_{l_j+2}/[\Lambda(l_j+1) - m\nu], \tag{A24}$$

where again the symbols have the same meanings as those of Lee & Saio (1987). Equations (A23) and (A24) constitute the final result, and are identical to the expressions found by Lee & Saio (1987) for even modes.

This paper has been typeset from a TEX/LATEX file prepared by the author.